

The effect of integral control in oscillatory and chaotic reaction kinetic networks

Kristian Thorsen^{a,*}, Tormod Drengstig^a, Peter Ruoff^b

^a*Department of Electrical Engineering and Computer Science, University of Stavanger, Norway*

^b*Centre for Organelle Research, University of Stavanger, Norway*

Abstract

Integral control is ubiquitously used in industrial processes to keep variables robustly regulated at a given setpoint. Integral control is also present in many biological systems where it, implemented through reaction kinetic networks of genes, proteins and molecules, protects the organism against external variations. One difference between industrial control systems and organisms is that oscillatory behavior seems to be more common in biology. This is probably because engineers can choose to design systems that avoid oscillations. Looking at regulation from the viewpoint of biological systems, the prevalence of oscillations leads to a question which is not often asked in traditional control engineering: how can regulatory and adaptive mechanisms function and coexist with oscillations? And furthermore: does integral control provide some kind of robust regulation in oscillatory systems? Here we present an analysis of the effect of integral control in oscillatory systems. We study nonlinear reaction kinetic networks where integral control is internally present and how these systems behave for parameter values that produce periodic and chaotic oscillations. In addition, we also study how the behavior of an oscillatory reaction kinetic network, the Brusselator, changes when integral control is added to it. Our results show that integral control, when internally present, in an oscillatory system robustly defends the average level of a controlled variable. This is true for both periodic and chaotic oscillations. Although we use reaction kinetic networks in our study, the properties we find are applicable to all systems that contains integral control.

Keywords: Reaction networks, Integral control, Chaos, Oscillations, Homeostasis

2010 MSC: 34C15, 34H10, 92C40, 92C42, 93C10, 93C15

Highlights

- Biological reaction kinetic networks can show oscillatory and chaotic behavior. 20
- We study the effect of integral control in systems that show oscillations. 5
- We show that integral control has a regulatory effect even during oscillations. 25
- We study the behavior of the Brusselator with and without added integral control. 10
- Integral action defends the average value in both periodic and chaotic oscillations. 30

1. Introduction

From a control engineering point of view it is clear that negative feedback with integral control is an attractive mechanism for providing robust regulation. Integral control is also common in biology. Many studies have indeed identified integral control to be internally present in

reaction kinetic networks of regulatory biochemical systems [1, 2, 3, 4], and there is an ongoing effort in synthetic biology to design integral control motifs that can be used in engineered cells [5, 6, 7]. However, because of practical constraints and limitations, biological controllers do most often not operate with the same mathematical simplicity and purity as man-made controllers in electromechanical systems [5, 6, 7, 8, 9].

Although the theory behind integral control is well established, not much work has been done on its effect in oscillatory systems. This may be because oscillations are traditionally avoided in man made control systems. It is relatively straightforward to design systems that don't oscillate, so why consider systems that do?

There are many biochemical systems that display oscillatory behavior [10, 11]. Examples include metabolic glycolysis [12, 13], circadian rhythms [14, 15], and synthetic genetic networks [16, 17, 18, 19]. Oscillatory behavior is also observed in pure chemical reactions like the Belousov-Zhabotinskii reaction [20, 21]. This reaction is often studied as a model for more complex biochemical processes, for instance in relation to synchronization of oscillations across unicellular populations [22, 23]. Most of the oscillatory systems in biology show periodic oscillations, but there are also systems that show irregular and chaotic oscillations under specific conditions [24, 25, 13]. Such

*Corresponding author

Email address: kristian.thorsen@uis.no (Kristian Thorsen)

chaotic behavior is seen in chemical oscillators [26, 27], enzyme-catalyzed reactions [28, 29], excitable cells [30, 31], and in glycolysis [32, 33]. In addition to experimental observations chaos has also been shown to exist in mathematical models of metabolic networks, for example in a model of glycolysis [33], and in a model of metabolism and redox balance in mitochondria [34].

In this work we study integral control in reaction kinetic networks and focus on regulation from the viewpoint of biochemical systems. The properties we find should however be generally applicable to all systems that contain integral control.

1.1. Integral control in reaction kinetic networks

We have previously presented a set of simple two component network motifs with structures that can provide integral control [4, 35]. Two such motifs are used in this study to examine how integral control affects oscillatory networks. An outflow controller (type 5 in [4]) is used here in the main text, and an inflow controller (type 2 in [4]) is used in the Supplementary Material (SM). The outflow controller is shown in Fig. 1a; the solid lines represent mass flow, and the dashed lines represent signaling. A chemical species A , called the controlled species, is regulated through negative feedback by a chemical species E , called the controller species. The controller species compensates for changes in A , caused by disturbance in the inflow (or outflow) of A , by adjusting a compensatory outflow $j = k_3AE/(K_M^A + A)$. The motif is called an outflow controller because it adjusts an outflow.

The change in E is described by the following rate equation

$$\dot{E} = k_5A - \frac{k_6E}{K_M^E + E}, \quad (1)$$

where the removal of E is described by a Michaelis-Menten expression. Integral control is most easily implemented by having zero-order removal of E with respect to itself, but other arrangements are also possible [36]. Assuming zero-order removal (saturation with $K_M^E \ll E$) the rate equation for E becomes

$$\dot{E} = -k_5 \left(\frac{k_6}{k_5} - A \right), \quad (2)$$

which is similar to the standard integral control law [35]. The equation for \dot{E} has A as its only variable, that is: $\dot{E} = h(A)$. The steady state condition, $h(A) = 0$, gives a simple expression for the defended level of A (the setpoint):

$$A_{set} = \frac{k_6}{k_5}. \quad (3)$$

The function of this controller motif can be illustrated by the block schematic representation in Fig. 1b. This representation, which is commonly used in control engineering, shows that the concentration of the controller E is the integrated difference (error) between the setpoint and the fed back measurement of A .

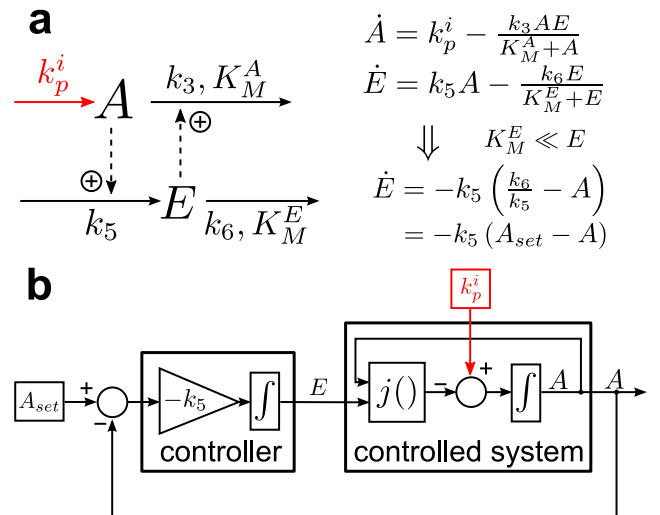


Figure 1: **Negative feedback outflow controller.** (a) Reaction network representation and rate equations for the motif. The controller variable E is activated by A and feeds back by adjusting the outflow of A . We treat a changing inflow of A through the parameter k_p^i as the primary disturbance to the system, see the text under section 2 Methods. (b) Control engineering type block schematic representation showing how the motif can be separated into a controller and a controlled system. The primary disturbance (k_p^i) is marked in red. The $j(\cdot)$ block represents how the controller (E) affects the controlled system (A), i.e., by a compensatory flow $j = k_3AE/(K_M^A + A)$.

2. Methods

We will use two different approaches to examine the effect of integral control in oscillatory reaction kinetic networks. The first approach (in sections 3.1 and 3.2) is to use a reaction kinetic network where integral control is already present, i.e., the controller motif from Fig. 1a., and extend/alter this network until oscillatory behavior appear. The second approach (in section 3.3) is to add integral control to an already oscillating system. For this we will use the oscillatory reaction kinetic network known as the Brusselator [37, 38] and add integral control in form of only the E -part from a controller motif, i.e., add Eq. 1 and an E -dependent outflow of the variable to be controlled.

The first approach can be thought of as similar to how oscillatory behavior may develop in existing regulatory reaction kinetic networks in cells and organisms, either through evolution, or through internal changes within a single organism. The second approach is more an engineer's approach where one has a system and then adds something to the system to see how it alters behavior. Since the system already oscillates this method makes it possible to see how the oscillatory behavior differs with and without integral control in the system.

We will throughout the work presented here use integral control motifs that act on the outflow of the species to be controlled. This is similar to an industrial controller that controls the level in a water tank by controlling an

actuator in the form of an outflow valve or an outflow pump. In other words, the actuator removes the controlled species, called A , from the system when it is in excess. Since the actuator is unable to add A to the system, i.e., provide a negative outflow, it is most suited to compensate for disturbances in the inflow to the system. We will thus treat parameters that changes the inflow of A as the main disturbances to the system.

Note that the situation is opposite for a reaction kinetic system where integral control is provided by an inflow controller motif (see SM6). A controller that compensates by adjusting an inflow is best suited to compensate against changes in outflow, i.e., disturbances in outflow. For a more detailed discussion about the differences between inflow and outflow controller motifs, what type of disturbances they are suited to compensate for, and what happens when disturbances that they are not fitted to compensate against start to dominate, we refer to our previous work in [4, 39].

Computations were performed by using Matlab (mathworks.com). Numerical integrations were done with the variable step stiff solver *ode15s* (supplied with Matlab). A relative tolerance of 10^{-9} , an absolute tolerance of 10^{-12} , and a maximum step size of 0.1 was specified as solver options. State variables (A , E , Z , etc.) will typically represent concentrations of chemical compounds.

The word equilibrium point is herein used to describe a constant solution to a system of differential equations, i.e., a point where $\dot{x}_i = 0$ for all i state variables.

2.1. A note on degree of perfectness

The term setpoint is herein used as the theoretical steady state value of A given perfect zero-order removal of E in the above controller motifs. In other words, under pure and perfect integral control. The removal will however never be exactly zero-order in real biochemical networks, i.e., K_M^E will have a value different from zero. This will shift the actual stationary value of a controller motif away from the theoretical setpoint. The difference between the setpoint and the actual stationary value is a measure of the controller's accuracy [4], or better put inaccuracy [39], and it is related to the value of the fraction $f(E)$ given as:

$$f(E) = \frac{E}{K_M^E + E}. \quad (4)$$

This fraction represents the degree of zero order removal of E , and thus the degree of perfect integral control. To exemplify, consider a stationary case where $E = 10$ and $K_M^E = 0.1$. Then $f(E) \approx 1$ and we have tight control (small inaccuracy). In another situation where $E = 0.4$ and $K_M^E = 0.1$, we get $f(E) = 0.8$ implying 20% deviation between A and A_{set} .

This inaccuracy can be almost impossible to detect if very low K_M^E values like 10^{-6} are used. We have in this study selected to use K_M^E values that makes the effect visible. See [4] and [40] for more details.

3. Results

We start the first approach with a motif that already contains integral control. The presented controller motif from Fig. 1a, and the rest of the complete set of motifs [4], can be extended to create systems that show sustained oscillations [41]. Such extensions can be done without changing the structure of the controller part (E), leaving a functional integral controller in the oscillating system.

3.1. Control of average concentration during periodic oscillations

Consider an oscillatory version of the outflow controller with added autocatalysis, shown in Fig. 2a. The equation for change in E is the same as before (Eq. 1), but the change in A is now described by:

$$\dot{A} = k_p^i + k_2 A - \frac{k_3 A E}{K_M^A + A}. \quad (5)$$

The rate constant k_p^i is still the inflow disturbance and k_2

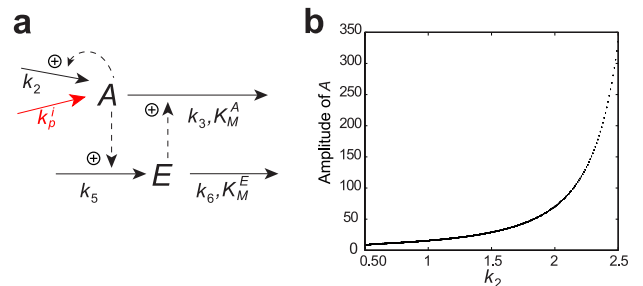


Figure 2: **A negative feedback outflow controller with oscillatory behavior.** (a) Outflow controller with autocatalysis in A (Eqs. 5 and 1). The controller variable E is activated by A and feeds back by adjusting the outflow of A . We treat a changing inflow of A , the parameter k_p^i , as the primary disturbance to the system. (b) Bifurcation diagram showing how the amplitude of the oscillations in A changes with the strength of autocatalysis k_2 . Parameters: $k_p^i=4$, $k_3=3.8$, $k_5=0.65$, $k_6=5.4$, $K_M^A=0.15$, and $K_M^E=0.5$. Initial conditions: $A_0=25.95$, $E_0=7.63$.

is the autocatalytic part. This motif oscillates for a wide range of parameter values. Stronger autocatalysis (higher k_2) leads to oscillations with greater amplitude. Figure 2b shows a bifurcation diagram of how the amplitude of the oscillations in A changes with the strength of autocatalysis.

Examples of the behavior in A and E for a stepwise change in k_p^i is shown in Figs. 3a and 3b. Interestingly the average of A , denoted $\langle A \rangle$ (black line in Fig. 3a), seems to be only transiently affected by the disturbance. We did several similar simulations/experiments to this and to other oscillating controller motifs, and they all indicated the same: The average level of A appears to be regulated. The results of a full sweep study of the average level of A versus the strength of inflow disturbance for this outflow motif is shown in Fig. S1 in SM1.

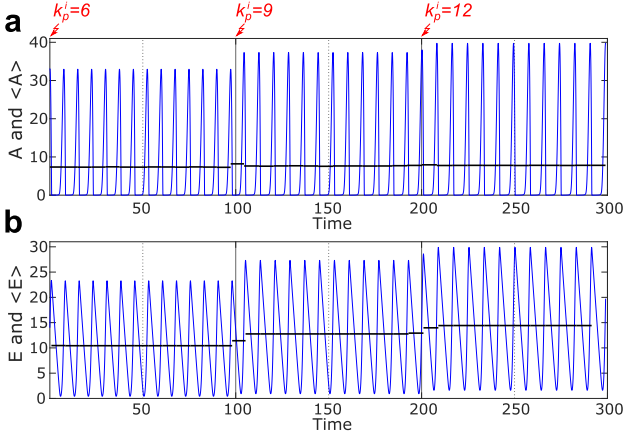


Figure 3: **Response to inflow disturbance changes in an oscillatory outflow controller.** (a) Oscillations in A shown for a stepwise inflow disturbance in k_p^i from 6 to 9 at $t=100$, and from 9 to 12 at $t=200$, as indicated. The black line shows the periodic average of A , calculated between peaks. Parameters: $k_2=1.5$, $k_3=3.8$, $k_5=0.65$, $k_6=5.4$, $K_M^A=0.15$, and $K_M^E=0.5$. Initial conditions: $A_0=33$, $E_0=14$. (b) Oscillations in and average of E during the same disturbance.

The general property of integral control, that a controller regulates A to a setpoint, is derived from the steady-state condition, $\dot{E} = h(A) = 0$. The steady-state condition can however not be used when the controllers are oscillating.

In order to derive the property of integral control during periodic oscillations we start by the definition of periodicity. For each repeating cycle E is back at exactly the same value

$$E(t+T) = E(t), \quad (6)$$

where T is the *period time*, the time of one cycle. The change in E cannot be assumed to be zero, as in nonoscillatory systems (steady state condition), but the integrated change in E over one period must be zero:

$$\int_t^{t+T} \dot{E} dt = E(t+T) - E(t) = 0. \quad (7)$$

This must also be the case for any integer number n of periods from t to $t+nT$. We now introduce the *periodic average* value of \dot{E} , denoted $\langle \dot{E} \rangle$, which must also be zero:

$$\langle \dot{E} \rangle \triangleq \frac{1}{T} \int_t^{t+T} \dot{E} dt = 0. \quad (8)$$

The rate equation of E for any motif can be inserted into Eq. 8. Inserting \dot{E} from Eq. 1 into Eq. 8 gives:

$$\langle \dot{E} \rangle = \frac{1}{T} \int_t^{t+T} \left(k_5 A - \frac{k_6 E}{K_M^E + E} \right) dt. \quad (9)$$

By applying zero-order kinetics, i.e., $K_M^E \rightarrow 0$, this reduces

to

$$\langle \dot{E} \rangle = k_5 \left(\frac{1}{T} \int_t^{t+T} A dt \right) - k_6 \left(\frac{1}{T} \int_t^{t+T} 1 dt \right) \quad (10)$$

$$= k_5 \left(\frac{1}{T} \int_t^{t+T} A dt \right) - k_6, \quad (11)$$

where the periodic average of A , denoted $\langle A \rangle$ can be identified. Using this and $\langle \dot{E} \rangle = 0$ (Eq. 8) we find that the controller maintains the periodic average of A at a setpoint which we term $\langle A \rangle_{set}$:

$$\langle A \rangle \triangleq \frac{1}{T} \int_t^{t+T} A dt = \frac{k_6}{k_5} = \langle A \rangle_{set}. \quad (12)$$

Note that this derivation also holds for nonoscillatory controller motifs. A system in steady state is a trivial solution of Eq. 6.

Similar to the stationary case (Eq. 3), the setpoint $\langle A \rangle_{set}$ in Eq. 12 is a theoretical setpoint that depends on $K_M^E \rightarrow 0$. The actual average $\langle A \rangle$ may thus differ somewhat from $\langle A \rangle_{set}$ at realistic conditions when K_M^E has a nonzero value (see section 2.1).

3.2. Controller action in the chaotic regime

We will in this section extend our results and look into the function of integral control in systems with sustained nonperiodic oscillations. To do this we will first show how systems based on the presented controller motifs can be extended from periodic to chaotic oscillating systems.

In systems of ordinary differential equations chaos can only appear if the system has a dimension of three or higher and only if at least one of the equations are nonlinear. These conditions do not, however, guarantee the presence of a chaotic solution. Even if we don't know all the necessary and sufficient conditions for chaos, the composition of chaotic systems in three dimensions is relatively well known [42, 43].

One way to build a system which should be able to show chaos, at least for some parameter values, is to combine a two dimensional oscillator with a switch; a type of structure first conceived by O. Rössler in some of the earliest studies of chaotic systems [44, 45]. The idea is best explained by the behavior in phase space. A trajectory spirals outwards from an unstable focus towards where the oscillator in two dimension would have formed an attractive limit cycle. Somewhere on this path the switch is activated and it lifts the trajectory up and into an area in phase space where the flow is reversed. The trajectory is then brought back down closer to the unstable focus than it was before it was lifted out. This is called *rejection* [44, 43]. For this to work the state variable defining the switch should have comparably fast dynamics, so that it creates a manifold in phase space that guides the movement of the other two oscillating state variables.

With this in mind we expanded the oscillating outflow controller (Fig. 2a) with an extra state variable Z that acts

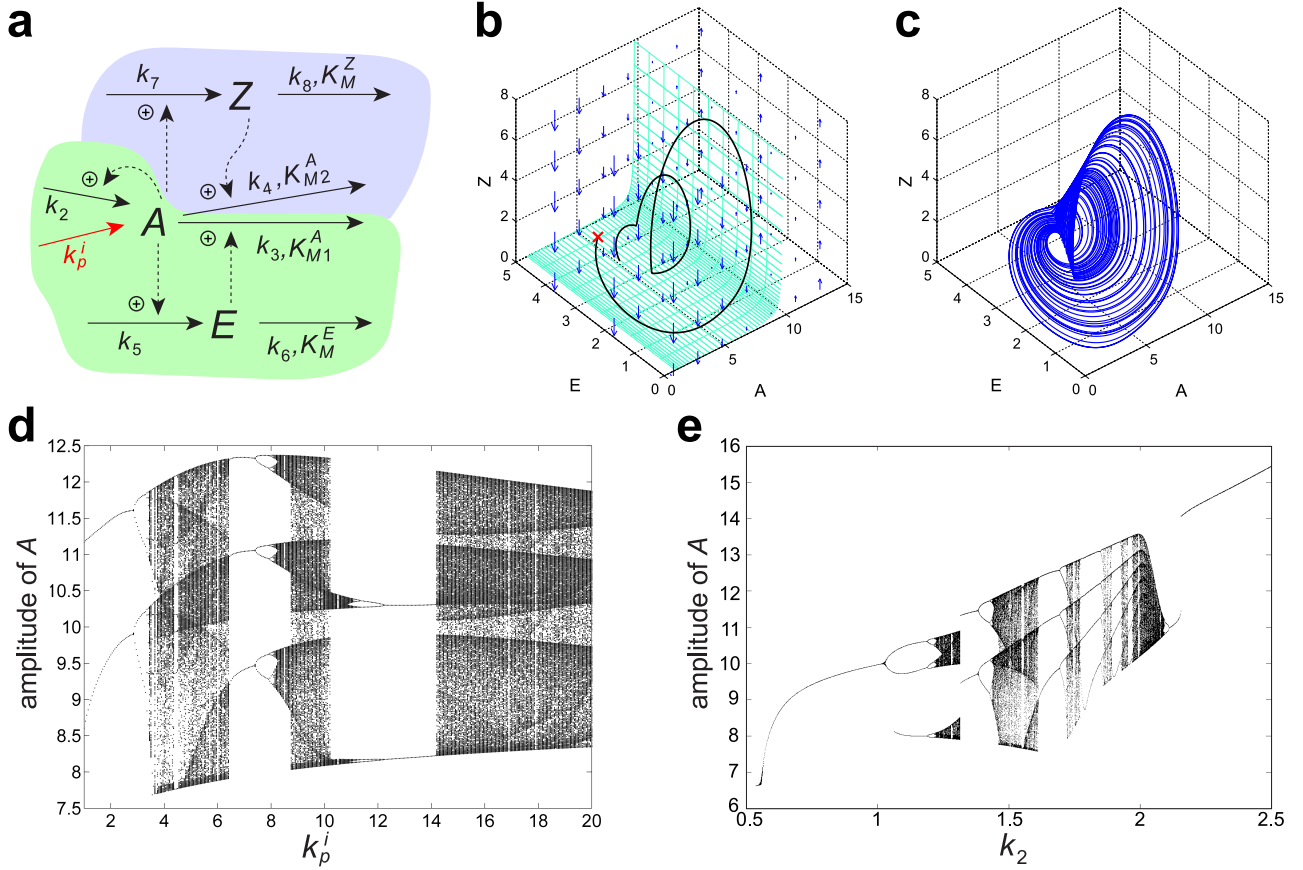


Figure 4: **Extended outflow controller capable of showing chaotic behavior.** (a) Chaotic outflow controller built by combing an oscillating controller (green, identical to Fig. 2a) with a switch (blue, made out of a negative feedback similar to the controller structure, but with faster dynamics). (b) Phase space with the manifold created by the fast dynamics of the Z -switch (given by Eq. 16). Blue arrows show the vector field of Z . A trajectory (in black) spiralling outwards from a focus point is reinjected, enabling the occurrence of chaos. Parameters: $k_p^i = 4$, $k_2 = 1.5$, $k_3 = 3.8$, $k_4 = 3.7$, $k_5 = 0.65$, $k_6 = 5.4$, $k_7 = 7.7$, $k_8 = 75$, $K_{M,1}^A = K_{M,2}^A = 0.15$, $K_M^E = 0.5$, and $K_M^Z = 0.03$. The trajectory starts in $[5.5, 4.5, 0.04]$ (red cross). (c) The chaotic attractor for this system shown in phase space. (d) Bifurcation diagram showing how the amplitude of the oscillations in A changes with disturbance in inflow k_p^i (other parameters as above). (e) Bifurcation diagram showing how the amplitude of the oscillations in A changes with the strength of the autocatalysis k_2 (other parameters as above). Simulations in (d) and (e) are run for 500 time units before collection of data to avoid transients.

as a single threshold switch. The reaction kinetic structure is shown in Fig. 4a where the original oscillating structure is colored in green and the new addition is colored in blue. The rate equations for this new motif are:

$$\dot{A} = k_p^i + k_2 A - \frac{k_3 A E}{K_{M,1}^A + A} - \frac{k_4 A Z}{K_{M,2}^A + A} \quad (13)$$

$$\dot{E} = k_5 A - \frac{k_6 E}{K_M^E + E} \quad (14)^{225}$$

$$\dot{Z} = k_7 A - \frac{k_8 Z}{K_M^Z + Z}. \quad (15)$$

The equation for Z is similar to E and is really just an extra negative feedback and outflow controller on A , but its dynamics is faster with relative high values on rate constants k_7 and k_8 .

The surface created by the fast dynamics of Z divides the phase space into two regions, shown in Fig. 4b. The

surface is given by

$$F_Z(A, E, Z) = k_7 A - \frac{k_8 Z}{K_M^Z + Z} = 0. \quad (16)$$

Figure 4b also illustrates how this system, for a certain set of parameters, shows reinjection. A trajectory starts to move on the horizontal part of the surface without much change in Z . When the oscillations cause the value of A to rise above a threshold at around $A = 10$ the switch is activated and the trajectory is lifted upwards in phase space by an increasing Z ; the trajectory is guided by the manifold. As Z increases \dot{A} is reduced (Eq. 13). Ultimately \dot{A} turns negative and we have reversed flow compared to the lower part of phase space. As A is reduced so is Z and the trajectory is reinjected into the horizontal part of the surface. This then repeats before the trajectory again starts to move on the horizontal part of the surface, only somewhat closer to the focus which it oscillates around. This behavior continues indefinitely; the trajectory moves

on a chaotic attractor as shown in Fig. 4c. A more detailed view of the direction of flow is given in Fig. S2 in SM2.

Whether the system displays this chaotic behavior or more simple periodic oscillations is dependent on the parameter values. As noted we are mainly interested in changes in behavior due to changes in inflow, and will thus focus on how the system responds to changes in the strength of autocatalysis k_2 and the disturbance k_p^i .

Figure 4d shows a bifurcation diagram for the amplitude of A for an increasing inflow disturbance, k_p^i , and Fig. 4e shows the same for increasing autocatalysis k_2 . These bifurcation diagrams reveal the characteristic period doubling route to chaos. Further studies of the chaotic attractor for this system, including Poincaré sections, first-return maps, and a movie or the movement of the attractor in phase space, is given in SM3.

The interesting questions are now: What happens with the average level of A during chaos? Will the integral action in E still provide robustness against disturbances in inflow? We first examined this by simulating the chaotic system for a range of different disturbances, and studied how the average level of A was affected. Before presenting the results we note that the definition of a periodic average $\langle A \rangle$ from Eq. 12 is not useful for chaotic systems since there is no defined period T . Instead of calculating the periodic average, we have calculated the average over a sufficiently long length of time τ as:

$$\langle A \rangle_\tau \triangleq \frac{1}{\tau} \int_{t_0}^{t_0+\tau} A dt. \quad (17)$$

The results from many simulations with k_p^i in the range from 4 to 40 are combined in Fig. 5, which shows the average level of A and E . We have here used $\tau = 50$ (what makes a sufficiently long τ is discussed towards the end of this section). The results indicate that the average level of A is still defended and that the presence of chaos does not alter the regulatory properties of the system. The average level of the controller species E increases with the level of the k_p^i disturbance. This makes sense from the structure of the reaction kinetic network, Fig. 4a; an increased inflow of A through k_p^i is compensated by an increased E -mediated outflow of A .

The response to stepwise changes in inflow disturbance (k_p^i) is shown in Fig. 6. The system is challenged with a step in k_p^i from a periodic region ($k_p^i = 13$) to a chaotic region ($k_p^i = 15$), and the controller responds by increasing the average level of E , which again increases the compensatory outflow of A . Fig. 6 also shows the response to a further step in the disturbance from $k_p^i = 15$ to $k_p^i = 20$.

Consequently, the integral controller E maintains the average level of A near the theoretical setpoint, as shown in Fig. 5. The average value of A is maintained even though the system moves in and out of chaotic behavior as the inflow disturbance changes. The system changes between chaotic and periodic behavior as indicated in the bifurcation diagram in Fig. 4d. The small difference between

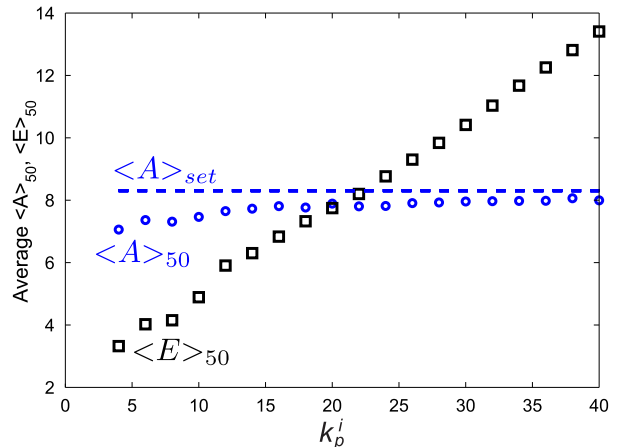


Figure 5: **Control of the average of A under chaotic conditions.** (a) Average level of A , $\langle A \rangle_{50}$ (blue circles), for the chaotic outflow controller in Fig. 4a (Eqs. 13-15) for different levels of inflow disturbances. The black squares show the average level of E , and the dashed blue line shows the theoretical setpoint of A , $\langle A \rangle_{set} = k_6/k_5 = 8.3$. The averages are calculated over a time length of $\tau = 50$. Parameters: $k_2 = 1.5$, $k_3 = 3.8$, $k_4 = 3.7$, $k_5 = 0.65$, $k_6 = 5.4$, $k_7 = 7.7$, $k_8 = 75$, $K_{M,1}^A = K_{M,2}^A = 0.15$, $K_M^E = 0.5$, and $K_M^Z = 0.03$. Initial conditions: $A_0 = 8.30$, $E_0 = 3.18$ and $Z_0 = 0.16$. Transient effects are avoided by letting simulations run for a time length of 100 before starting the calculation of averages.

$\langle A \rangle_\tau$ and the theoretical setpoint can be attributed to the level of E and the parameter K_M^E . Higher level of E means that its removal becomes more saturated, hence the $f(E)$ fraction (Eq. 4) is closer to 1 and the controller becomes more accurate, see also section 2.1.

Analytically deriving the properties of integral control during chaotic conditions may not seem as straightforward as in the periodic case. We can no longer use periodicity as we did in Eqs. 6–12. The integrated change of E from a point in time t_0 to a point in time $t_0 + \tau$ will for an arbitrary value of τ be equal to some number ϵ , which is the difference between $E(t_0 + \tau)$ and $E(t_0)$. That is:

$$\int_{t_0}^{t_0+\tau} \dot{E} dt = E(t_0 + \tau) - E(t_0) = \epsilon. \quad (18)$$

For a system with a chaotic attractor we have that ϵ is bounded when $\tau \rightarrow \infty$, given that the trajectory is on the attractor at time t_0 (transients have died out). A trajectory already on a chaotic attractor (after transients) will forever move on the attractor, and thus $E(t_0 + \tau)$ cannot move further away from $E(t_0)$ than the extent of the attractor along the E -axis in phase space.

Taking the time average of \dot{E} as in Eq. 17 we have that:

$$\langle \dot{E} \rangle_\tau = \frac{1}{\tau} \int_{t_0}^{t_0+\tau} \dot{E} dt = \frac{\epsilon}{\tau}. \quad (19)$$

By continuing the derivation as in Eqs. 8–12 we find that integral control (implemented by zero-order kinetics) de-

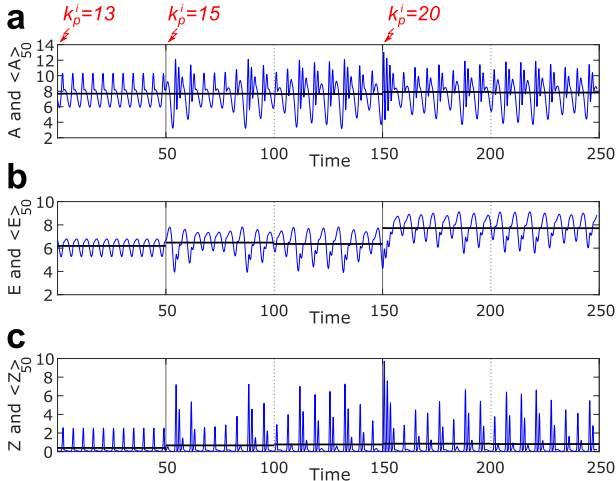


Figure 6: **Example response for the chaotic outflow controller to a stepwise change in inflow.** (a) Response to an inflow disturbance given as a stepwise change for the chaotic outflow controller in Fig. 4a (Eqs. 13-15). The disturbance k_p^i is stepped from 13 to 15 at $t=50$, and from 15 to 20 at $t=150$, as indicated. The level of A is shown in blue while the average of A , $\langle A \rangle_{50}$, is shown in black. (b) Level and average of E . (c) Level and average of Z . Parameters: $k_2=1.5$, $k_3=3.8$, $k_4=3.7$, $k_5=0.65$, $k_6=5.4$, $k_7=7.7$, $k_8=75$, $K_{M,1}^A=K_{M,2}^A=0.15$, $K_M^E=0.5$, and $K_M^Z=0.03$. Initial conditions: $A_0=6.91$, $E_0=6.65$ and $Z_0=0.07$. The averages are calculated over fixed intervals with a length of $\tau=50$ starting from $t=0$ to $t=50$, from $t=50$ to $t=100$, and so on.

fends the average level of the controlled variable A at:

$$\langle A \rangle_\tau = \frac{1}{\tau} \int_{t_0}^{t_0+\tau} A dt = \frac{k_6}{k_5} + \frac{\epsilon}{k_5 \tau}. \quad (20)$$

Furthermore when $\tau \rightarrow \infty$, this reduces to the same theoretical setpoint as in the periodic case (Eq. 12), that is:

$$\lim_{\tau \rightarrow \infty} \langle A \rangle_\tau = \frac{k_6}{k_5} = \langle A \rangle_{set}. \quad (21)$$

This proves that integral control provides robust regulation even when the system behaves chaotically.

In practice τ does not have to go to infinity; it is sufficient to have τ large enough to make the contribution from ϵ negligible. From our experience it is enough to have a τ value that allows the trajectory to cover most of the attractor. Around 10 times the quasi-period, or 10 times around the attractor, is usually sufficient.

It is possible to relate the setpoint of $\langle A \rangle_\tau$ and the behavior of $\langle E \rangle_\tau$ seen in Fig. 5 to an unstable equilibrium point of the overall system. This is shown in SM4 and discussed further in the next section where we add integral control to an already oscillating system.

The above method for calculating the average of a variable is convenient as it works well for stationary, periodic, and chaotic behavior without much need for prior information about how the system behaves or the shape and position of the attractor in phase space. An alternative approach that is arguably more mathematical elegant, and

equivalent to the periodic average, is to calculate the average between two successive intersections with a Poincaré section. This method is used in SM5 to calculate the averages during a change in inflow disturbance in the chaotic outflow controller (the same experiment as in Fig. 6), and the method gives similar results. However elegant, this method is more cumbersome as it requires prior information about the attractor in order to choose a fitting placement of the Poincaré section.

3.3. Adding integral control to an already oscillating reaction kinetic network

In the preceding parts we started with a reaction kinetic network that already contained an integral controller, and extended this system to show its behavior under periodic and chaotic oscillations. We will now take a different approach by starting with an oscillatory reaction kinetic network that does not contain integral control, and study how its behavior changes when integral control is added to the system.

The Brusselator is a widely studied theoretical reaction kinetic network that shows limit cycle oscillations. It was proposed by Lefever, Nicolis and Prigogine and is named after the city of Brussels where they were based [37, 38]. The Brusselator can be expressed with two chemical species, X and Y , having the following rate equations [38, 46]:

$$\dot{X} = k_p^i - k_2 X + k_3 X^2 Y - k_4 X \quad (22)$$

$$\dot{Y} = k_2 X - k_3 X^2 Y. \quad (23)$$

A reaction network representation of the Brusselator is shown in Fig. 7a (do not consider the green part yet). To illustrate the effect of integral control we have selected to treat the independent inflow of X as a disturbance to the system, i.e., we let the rate constant k_p^i vary. The Brusselator system has *one* equilibrium point,

$$X^* = \frac{k_p^i}{k_4}, \quad Y^* = \frac{k_2 k_4}{k_p^i k_3}, \quad (24)$$

that may be stable or unstable depending on the value of the rate constants. When the equilibrium is unstable the system has a stable limit cycle that gives rise to periodic oscillations. Note that the equilibrium value of X is dependent on the amount of inflow of X through the reaction described by the disturbance k_p^i .

The goal here is not to give a thorough examination of the stability and behavior of the Brusselator, which has been done elsewhere [47, 48, 38, 46], but to look at how its behavior changes when an integral controller is added to the system.

The response of the Brusselator to stepwise changes in the disturbance k_p^i is shown in Figs. 7b and 7c. For the parameter values that we use (listed in the caption of Fig. 7) we see that the Brusselator is stable and that there are steady state solutions for $k_p^i = 0.5$ and $k_p^i = 0.3$.

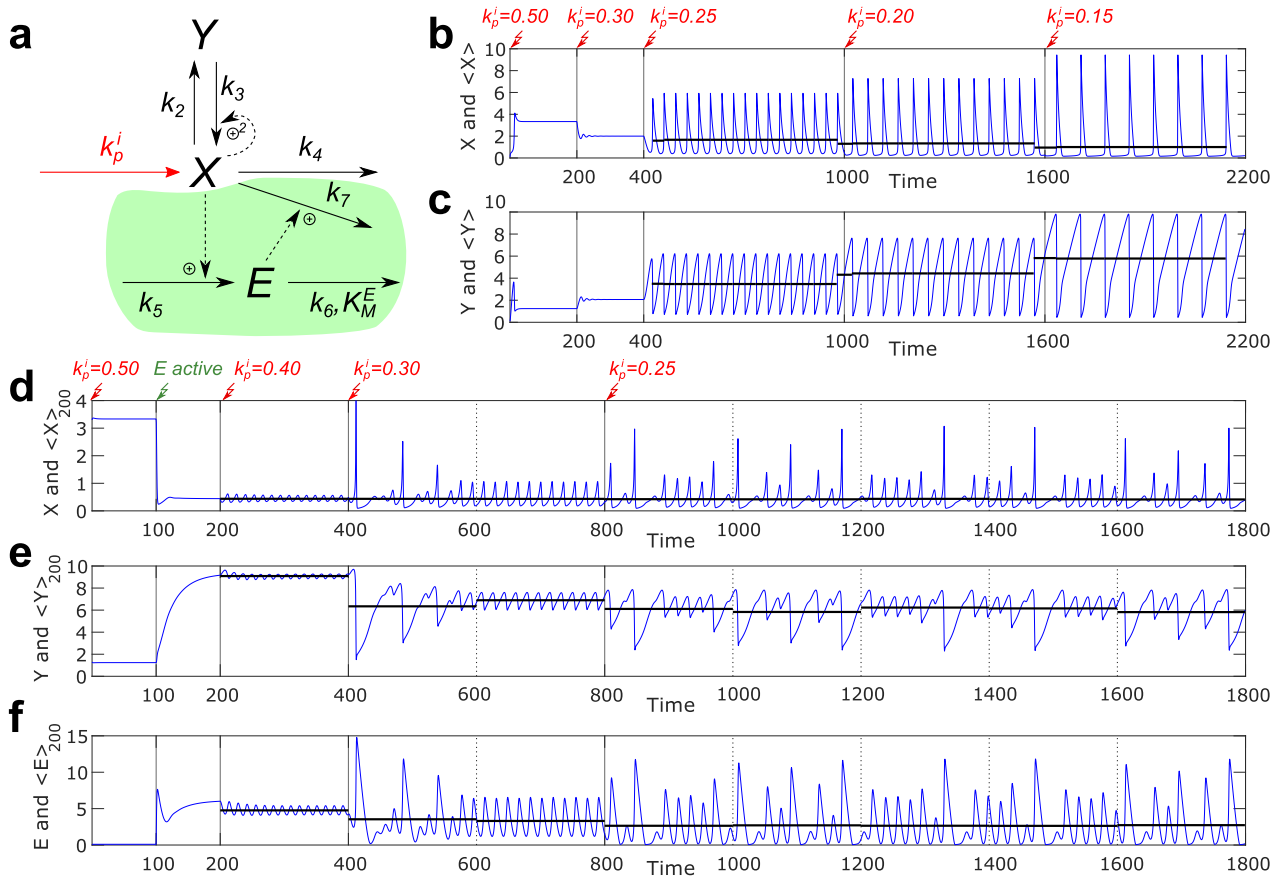


Figure 7: **Behavior of the Brusselator with and without added integral control.** (a) Brusselator (white background) and an added outflow controller motif (green background) that provides integral control of X . The system behavior will be analyzed for varying production of X , i.e., the k_p^i parameter is treated as a disturbance. (b) and (c) Behavior of the pure Brusselator, Eqs. 22–23 (without added integral control). The plots show the concentration of the chemical species X and Y in blue for different values of the disturbance k_p^i . The periodic average is plotted in black when the system oscillates. The disturbance k_p^i is changed from 0.5 to 0.15 in steps at the times indicated in the figure. Parameters: $k_2=0.95$, $k_3=0.23$, $k_4=0.15$. Initial conditions: $X_0=Y_0=0.1$. (d)–(f) Behavior of the Brusselator with added integral control, Eqs. 25–27 (from $t=100$). The plots show the concentration X , Y , and E in blue, in addition to the average of these variables in black calculated over fixed intervals with a length of $\tau=200$ starting from $t=200$ to $t=400$, from $t=400$ to $t=600$, and so on. The controller is activated at $t=100$ by changing the value of parameters k_5 to k_7 from zero to their value listed in the following. The disturbance k_p^i is changed from 0.5 to 0.25 in steps at the times indicated in the figure. Parameters: $k_2=0.95$, $k_3=0.23$, $k_4=0.15$, $k_5=2.7$, $k_6=1.2$, $k_7=0.16$, and $K_M^E = 0.03$. Initial conditions: $X_0=3.3$, $Y_0=1.3$, $E_0=0.1$.

345 The Brusselator starts to oscillate when k_p^i is stepped from 0.3 to 0.25. The simulation results show that the value of X (and Y) during steady state and the periodic average $\langle X \rangle$ (and $\langle Y \rangle$) during oscillations change with varying disturbance values, as expected from Eq. 24.

Consider now that we want to control the (average) value of X in the Brusselator by adding an integral controller in the form of the controller motif marked with green in Fig. 7a. The extended equations for this controlled Brusselator are:

$$\dot{X} = k_p^i - k_2X + k_3X^2Y - k_4X - k_7XE \quad (25)$$

$$\dot{Y} = k_2X - k_3X^2Y \quad (26)$$

$$\dot{E} = k_5X - \frac{k_6E}{K_M^E + E}. \quad (27)$$

The key point now is that the integral controller changes the equilibrium value of X , making it independent of the

parameters in the original Brusselator. As in Eqs. 3, 12, and 21 the controller introduces a setpoint for X at k_6/k_5 , which is only dependent on the parameters in the controller part of the system. The new equilibrium point is (assuming $K_M^E \ll E$):

$$X^* = \frac{k_6}{k_5}, \quad Y^* = \frac{k_2k_5}{k_3k_6}, \quad E^* = \frac{k_p^ik_5 - k_4k_6}{k_6k_7}. \quad (28)$$

Given the previous results from sections 3.1 and 3.2 we should now expect that the integral controller does not only hold X at the setpoint for parameters where the equilibrium is stable, but also that it for parameters that cause the system to oscillate (periodic or chaotic) keeps the *average value* of X at the setpoint. Simulation results shown in Figs. 7d to 7f confirm that this indeed is the case. When the controller is activated (at $t = 100$ in Fig. 7d) the value of X is moved from 3.33 (k_p^i/k_4) to the setpoint of the

controller at 0.44 (k_6/k_5). The controller then defends the
360 setpoint as the disturbance k_p^i is changed. The system
with integral control starts to oscillate as k_p^i is reduced to
0.4 (at $t = 200$ in Fig. 7d) and to 0.3, but the average level⁴¹⁵
of X is, apart from some transient behavior, kept at the
setpoint. This is also the case when the system displays
365 chaotic oscillations, as seen with a k_p^i of 0.25 (from $t = 800$
in Fig. 7d).

The introduction of an integral controller seems to make⁴²⁰
the solutions of the combined system less stable, or more
oscillatory, than for the system without added control. We
370 see that a lesser change in k_p^i is needed to induce oscil-
lations. This makes sense as an integral controller from
linear theory is known to reduce the stability margin of⁴²⁵
a system by causing phase lag. Nevertheless, the integral
controller provides a controlling effect during oscillations
375 in that it keeps the average level of A at a defined setpoint
independent of disturbances.

4. Discussion ⁴³⁰

Our results show the ability of integral control, imple-
380 mented by reaction kinetics, to regulate the average level
of a controlled variable in systems showing either periodic
or chaotic oscillations. ⁴³⁵

4.1. The controller motif and integral control

All the examples presented here use the same outflow
controller motif (type 5 in [4]). The motif essentially pro-
385 vides a setpoint for the controlled variable, and acts as⁴⁴⁰
an integral controller that changes the value of the con-
troller variable E until the controlled variable (A , or X)
is equal to the setpoint. A key feature is that the setpoint
only depends on parameters related to the kinetics of the
390 controller species E itself; it is independent of the parame-⁴⁴⁵
ters of the surrounding system that the controller controls.
This means that if we are able to add a controller motif to
an already existing reaction kinetic network, for example
by use of gene editing and synthetic biology, we can, at
395 least as far as the practical methods allow, design it to⁴⁵⁰
have the setpoint we want [4, 8].

What the setpoint really is, and what integral control
manifests itself as in the combined process-controller sys-
400 tem, is an equilibrium point where the controlled variable
has the value of the setpoint. This is clearly demonstrated⁴⁵⁵
by the addition of integral control to the Brusselator in
section 3.3. The equilibrium of X is moved from a point
dependent on the parameters of the Brusselator system,
 k_p^i/k_4 (Eq. 24), to a point dependent on the parameters of
405 the controller system, k_6/k_5 (Eq. 28). It is from this easy⁴⁶⁰
to understand how integral control in the case when the
equilibrium is stable provides setpoint tracking, and dis-
turbance rejection against disturbances in any parameters
apart from k_5 and k_6 .

410 However, although adding integral control provides a
new (controllable) equilibrium point, there is no guarantee

about the reachability and stability of this point. What
our results show here is the effect integral control has
when the equilibrium point it provides is unstable and en-
closed by a limit cycle or a chaotic attractor. Our results
show that integral control in this case keeps the average
level of the controlled variable equal to the value it has in
the unstable equilibrium point (setpoint). Mathematically
speaking, if the controlled variable is X then the integral
controller fixes the X coordinate position of the attrac-
tor in state space. Disturbance rejection for the average
level of the controlled variable readily follows, because the
value of the controlled variable in the unstable equilibrium
point still depends only on the controller parameters (k_5
and k_6).

4.2. Oscillations, chaos, and steady states

Robust control of the average level of a variable can
be seen as a generalization of the well known steady state
property of integral control, as the average level and the
steady state level are overlapping for nonoscillatory sys-
tems. The steady state condition, i.e., assuming steady
state by setting the derivatives equal to zero, is normally
used to derive the property of integral control. This con-
dition cannot be used directly when the system, which
the integral controller is a part of, shows oscillatory be-
havior. Nevertheless, as long as there is an attractor, en-
closing the unstable equilibrium point, that attracts and
confines the trajectories, the system is still in what we can
call a stable regime. The trajectories are not diverging,
but bounded with repetitive (although not always exactly
predictable) behavior. Seen from its outside borders the
attractor behaves just like an asymptotically stable equi-
librium point. The conditions we have used in Eqs. 7 and
19 can be viewed as an extension, or replacement, of the
steady state condition. The condition in Eq. 7 can be used
for systems that show periodic oscillations; and it can also
be used for nonoscillatory systems, for which it becomes
the same as the ordinary steady state condition. Likewise,
the condition in Eq. 19 can be used for chaotic, periodic,
and ordinary nonoscillatory systems.

While the ability to robustly defend an average value
is exciting, there are some caveats. Disturbances do not
change the average value, but they do change the ampli-
tude and frequency of the oscillations. The variations in
amplitude is clearly seen in the two bifurcations plots in
Figs. 4d and 4e for the chaotic outflow controller. For ex-
ample a k_2 of 0.6 and 2.4 both produce simple periodic
oscillations with the same average value of A , but with
almost a twofold difference in amplitude.

4.3. Biological significance

According to the classical concept by Cannon, homeo-
stasis keeps the concentrations of certain compounds within
tolerable limits and thereby contributes to the internal sta-
bility of cells and organisms [49]. Our results explain how

465 integral control enables biological systems to maintain ro-
bust homeostasis in the average, even when they show pe-
riodic or chaotic behavior. In other words it shows that
internal regulation against external disturbances (param-
eter changes) can be maintained even when systems are
470 oscillating. Integral control provides an active regulatory
mechanism that extends beyond just the stability of the
attractor.

Some may argue that the concepts of chaos and home-
ostasis appear incompatible even though there are exam-
475 ples of chaotic behavior in biological systems [50, 51, 52].
On one hand we have homeostasis as a mechanism to
achieve adaptation and stability (and some would argue
constancy), while on the other hand chaos is generally as-
sociated with processes which look unpredictable and ran-
480 dom. In the end the question of whether a chaotic system
with internal integral control can be said to be homeostat-
ically regulated is a question of whether to strictly define
homeostasis as only constancy. Such a strict definition has
before lead to new concepts like homeodynamics being in-
485 troduced to cover the broader range of regulatory behavior
[52]. However, instead of dividing it all up, it may more
constructive to generalize and extend the concept of home-
ostasis to include regulatory networks with oscillatory and
chaotic behavior [53].

Oscillatory behavior is, as mentioned in the introduc-
490 tion, quite common in biological systems. One explanation
for this is that regulatory networks that provide adapta-
tion and control with very small modifications can be made
to show oscillatory behavior. The evolutionary step from
495 an adapting reaction kinetic network to a oscillating one
is small. Evolutionary processes may have modified reac-
tion kinetic networks in a way that opens up for oscilla-
tions without necessarily having them display this behav-
ior right away. Organisms may then, by further evolution,
500 have evolved signalling mechanisms based on oscillations
of regulated compounds.

The step from simple periodic oscillations to chaotic os-
cillations also seems to be within relatively easy evolution-
505 ary reach, as illustrated by the presented reaction kinetic
networks. New interconnections and feedbacks are created
as organisms evolve to become more complex. Similar to
the here presented networks, the presence of multi-looped
negative feedbacks have been known to enhance complex
and chaotic dynamics [54, 55, 11]. Our results indicate
510 that such behavior can exist side by side with homeostasis;
active regulation by integral control defends homeostasis
even under oscillatory and chaotic conditions by keeping
the average level under control.

Acknowledgments

515 This research was financed in part by Program Area
Funds from the University of Stavanger.

Declaration of interest

Declaration of interests: none.

Supplementary Material

Supplementary text and movies. SM1-SM4: Further
studies on the outflow motif, including illustrations of the
flow in phase space and reinjection, a movie showing Poincaré
sections, first-return maps, and movement of the attractor
in phase space. SM5: Averaging over successive intersec-
tions of a Poincaré section. SM6-SM7: Study showing the
same regulatory effect of integral control, but with a differ-
ent inflow motif as example. SM8: An example showing
control of the average level of A for a motif with spiky
chaotic behavior.

References

- [1] T. Yi, Y. Huang, M. Simon, J. Doyle, Robust perfect adaptation in bacterial chemotaxis through integral feedback control, *Proc Natl Acad Sci USA* 97 (9) (2000) 4649–4653. doi:10.1073/pnas.97.9.4649.
- [2] J. Stelling, U. Sauer, Z. Szallasi, F. J. Doyle, J. C. Doyle, Robustness of cellular functions., *Cell* 118 (6) (2004) 675–685. doi:10.1016/j.cell.2004.09.008.
- [3] D. Muzzey, C. A. Gómez-Urbe, J. T. Mettetal, A. van Oudenaarden, A systems-level analysis of perfect adaptation in yeast osmoregulation., *Cell* 138 (1) (2009) 160–71. doi:10.1016/j.cell.2009.04.047.
- [4] T. Drengstig, I. W. Jolma, X. Y. Ni, K. Thorsen, X. M. Xu, P. Ruoff, A Basic Set of Homeostatic Controller Motifs, *Biophys J* 103 (9) (2012) 2000–2010. doi:10.1016/j.bpj.2012.09.033.
- [5] D. Del Vecchio, A. J. Dy, Y. Qian, Control theory meets synthetic biology, *J R Soc Interface* 13 (120) (2016) 20160380. doi:10.1098/rsif.2016.0380.
- [6] Z. F. Tang, D. R. McMillen, Design principles for the analysis and construction of robustly homeostatic biological networks, *J Theor Biol* 408 (2016) 274–289. doi:10.1016/j.jtbi.2016.06.036.
- [7] C. Briat, A. Gupta, M. Khammash, Antithetic Integral Feedback Ensures Robust Perfect Adaptation in Noisy Bimolecular Networks, *Cell Syst* 2 (1) (2016) 15–26. doi:10.1016/j.cels.2016.01.004.
- [8] J. Ang, D. R. McMillen, Physical constraints on biological integral control design for homeostasis and sensory adaptation., *Biophys J* 104 (2) (2013) 505–515. doi:10.1016/j.bpj.2012.12.015.
- [9] F. Mairet, A biomolecular proportional integral controller based on feedback regulations of protein level and activity, *R Soc Open Sci* 5 (2) (2018) 171966. doi:10.1098/rsos.171966.
- [10] A. Goldbeter, Computational approaches to cellular rhythms., *Nature* 420 (6912) (2002) 238–245. doi:10.1038/nature01259.
- [11] B. Novák, J. J. Tyson, Design principles of biochemical oscillators., *Nat Rev Mol Cell Biol* 9 (12) (2008) 981–991. doi:10.1038/nrm2530.
- [12] A. Boiteux, A. Goldbeter, B. Hess, Control of oscillating glycolysis of yeast by stochastic, periodic, and steady source of substrate: A model and experimental study, *Proc Natl Acad Sci USA* 72 (10) (1975) 3829–3833. doi:10.1073/pnas.72.10.3829.
- [13] P. Richard, The rhythm of yeast, *FEMS Microbiol Rev* 27 (4) (2003) 547–557. doi:10.1016/S0168-6445(03)00065-2.
- [14] J. C. Dunlap, J. J. Loros, Making Time: Conservation of Biological Clocks from Fungi to Animals, *Microbiol Spectr* 5 (3) (2017) 1–19. doi:10.1128/microbiolspec.FUNK-0039-2016.

- [15] I. Mihalcescu, W. Hsing, S. Leibler, Resilient circadian oscillator revealed in individual cyanobacteria, *Nature* 430 (6995) (2004) 81–85. doi:10.1038/nature02533.
- [16] M. B. Elowitz, S. Leibler, A synthetic oscillatory network of transcriptional regulators., *Nature* 403 (6767) (2000) 335–338. doi:10.1038/35002125.
- [17] J. Hasty, M. Dolnik, V. Rottschäfer, J. J. Collins, Synthetic gene network for entraining and amplifying cellular oscillations, *Phys Rev Lett* 88 (14) (2002) 148101/1–148101/4. doi:10.1103/PhysRevLett.88.148101.
- [18] J. Stricker, S. Cookson, M. R. Bennett, W. H. Mather, L. S. Tsimring, J. Hasty, A fast, robust and tunable synthetic gene oscillator, *Nature* 456 (7221) (2008) 516–519. doi:10.1038/nature07389.
- [19] Y. Chen, J. K. Kim, A. J. Hirning, K. Josić, M. R. Bennett, Emergent genetic oscillations in a synthetic microbial consortium, *Science* 349 (6251) (2015) 986–989. doi:10.1126/science.aaa3794.
- [20] R. J. Field, E. Körös, R. M. Noyes, Oscillations in chemical systems. II. Thorough analysis of temporal oscillation in the bromate-cerium-malonic acid system, *J Am Chem Soc* 94 (25) (1972) 8649–8664. doi:10.1021/ja00780a001.
- [21] J. C. Roux, A. Rossi, S. Bachelart, C. Vidal, Experimental observations of complex dynamical behavior during a chemical reaction, *Physica D* 2 (2) (1981) 395–403. doi:10.1016/0167-2789(81)90018-X.
- [22] A. F. Taylor, M. R. Tinsley, F. Wang, Z. Huang, K. Showalter, Dynamical quorum sensing and synchronization in large populations of chemical oscillators, *Science* 323 (5914) (2009) 614–617. doi:10.1126/science.1166253.
- [23] A. F. Taylor, M. R. Tinsley, K. Showalter, Insights into collective cell behaviour from populations of coupled chemical oscillators, *Phys Chem Chem Phys* 17 (17) (2015) 20047–20055. doi:10.1039/c5cp01964h.
- [24] B. Hess, M. Markus, Order and chaos in biochemistry, *Trends Biochem Sci* 12 (1987) 45–48. doi:10.1016/0968-0004(87)90024-7.
- [25] K.-P. Yip, D. Marsh, N.-H. Holstein-Rathlou, Evidence of low-dimensional chaos in renal blood flow control in genetic and experimental hypertension, *Physica D* 80 (1-2) (1995) 95–104. doi:10.1016/0167-2789(95)90063-2.
- [26] F. Argoul, A. Arneodo, P. Richetti, J. C. Roux, H. L. Swinney, Chemical chaos: from hints to confirmation, *Acc Chem Res* 20 (12) (1987) 436–442. doi:10.1021/ar00144a002.
- [27] J. C. Roux, R. H. Simoyi, H. L. Swinney, Observation of a strange attractor, *Physica D* 8 (1-2) (1983) 257–266. doi:10.1016/0167-2789(83)90323-8.
- [28] L. F. Olsen, H. Degn, Chaos in an enzyme reaction, *Nature* 267 (1977) 177–178. doi:10.1038/267177a0.
- [29] T. Geest, C. G. Steinmetz, R. Larter, L. F. Olsen, Period-doubling bifurcations and chaos in an enzyme reaction, *J Phys Chem* 96 (14) (1992) 5678–5680. doi:10.1021/j100193a004.
- [30] M. Guevara, L. Glass, A. Shrier, Phase locking, period-doubling bifurcations, and irregular dynamics in periodically stimulated cardiac cells, *Science* 214 (4527) (1981) 1350–1353. doi:10.1126/science.7313693.
- [31] L. F. Olsen, H. Degn, Chaos in biological systems, *Q Rev Biophys* 18 (2) (1985) 165–225. doi:10.1017/S0033583500005175.
- [32] M. Markus, D. Kuschmitz, B. Hess, Chaotic dynamics in yeast glycolysis under periodic substrate input flux, *FEBS Lett* 172 (2) (1984) 235–238. doi:10.1016/0014-5793(84)81132-1.
- [33] K. Nielsen, P. G. Sørensen, F. Hynne, H.-G. Busse, Sustained oscillations in glycolysis: an experimental and theoretical study of chaotic and complex periodic behavior and of quenching of simple oscillations, *Biophys Chem* 72 (1) (1998) 49–62. doi:10.1016/S0301-4622(98)00122-7.
- [34] J. M. Kembro, S. Cortassa, D. Lloyd, S. J. Sollott, M. A. Aon, Mitochondrial chaotic dynamics: Redox-energetic behavior at the edge of stability, *Sci Rep* 8 (1) (2018) 1–11. doi:10.1038/s41598-018-33582-w.
- [35] K. Thorsen, T. Drenstgig, P. Ruoff, Control theoretic properties of physiological controller motifs, in: ICSSE 2013, IEEE International Conference on System Science and Engineering, Budapest, 2013, pp. 165–170. doi:10.1109/ICSSE.2013.6614653.
- [36] T. Drenstgig, X. Y. Ni, K. Thorsen, I. W. Jolma, P. Ruoff, Robust adaptation and homeostasis by autocatalysis, *J Phys Chem B* 116 (18) (2012) 5355–5363. doi:10.1021/jp3004568.
- [37] I. Prigogine, R. Lefever, Symmetry breaking instabilities in dissipative systems. II, *J Chem Phys* 48 (4) (1968) 1695–1700. doi:10.1063/1.1668896.
- [38] J. J. Tyson, Some further studies of nonlinear oscillations in chemical systems, *J Chem Phys* 58 (9) (1973) 3919–3930. doi:10.1063/1.1679748.
- [39] K. Thorsen, Controller Motifs for Homeostatic Regulation and Their Applications in Biological Systems, PhD thesis, University of Stavanger, 2015.
- [40] G. B. Risvoll, K. Thorsen, P. Ruoff, T. Drenstgig, Variable setpoint as a relaxing component in physiological control, *Physiol Rep* 5 (17) (2017) e13408. doi:10.14814/phy2.13408.
- [41] K. Thorsen, O. Agafonov, C. H. Selstø, I. W. Jolma, X. Y. Ni, T. Drenstgig, P. Ruoff, Robust concentration and frequency control in oscillatory homeostats, *PLoS ONE* 9(9) (2014) e107766. doi:10.1371/journal.pone.0107766.
- [42] C. Letellier, E. Roulin, O. E. Röessler, Inequivalent topologies of chaos in simple equations, *Chaos, Solitons and Fractals* 28 (2) (2006) 337–360. doi:10.1016/j.chaos.2005.05.036.
- [43] C. Letellier, *Chaos in Nature*, World Scientific Series on Non-linear Science, Series A – Vol. 81 (ch. 4), World Scientific Publishing Co. Pte. Ltd., Singapore, 2013.
- [44] O. E. Röessler, Chaotic behavior in simple reaction systems, *Zeitschrift für Naturforschung A* 31 (3-4) (1976) 259 – 264. doi:10.1515/zna-1976-3-408.
- [45] O. E. Röessler, Chaos in abstract kinetics: Two prototypes, *Bull Math Biol* 39 (2) (1977) 275–289. doi:10.1007/BF02462866.
- [46] R. Lefever, G. Nicolis, P. Borckmans, The Brusselator: It does oscillate all the same, *J Chem Soc, Faraday Trans 1* 84 (4) (1988) 1013–1023. doi:10.1039/F19888401013.
- [47] R. Lefever, G. Nicolis, Chemical instabilities and sustained oscillations, *J Theor Biol* 30 (2) (1971) 267–284. doi:10.1016/0022-5193(71)90054-3.
- [48] B. Lavenda, G. Nicolis, M. Herschkowitz-Kaufman, Chemical instabilities and relaxation oscillations, *J Theor Biol* 32 (2) (1971) 283–292. doi:10.1016/0022-5193(71)90166-4.
- [49] W. Cannon, Organization for Physiological Homeostatics, *Physiol Rev* 9 (1929) 399–431. doi:10.1152/physrev.1929.9.3.399.
- [50] A. L. Goldberger, Is the Normal Heartbeat Chaotic or Homeostatic?, *Physiology* 6 (2) (1991) 87–91. doi:10.1152/physiologyonline.1991.6.2.87.
- [51] T. Elbert, W. J. Ray, Z. J. Kowalik, J. E. Skinner, K. E. Graf, N. Birbaumer, Chaos and physiology: deterministic chaos in excitable cell assemblies, *Physiol Rev* 74 (1) (1994) 1–47. doi:10.1152/physrev.1994.74.1.1.
- [52] D. Lloyd, M. Aon, S. Cortassa, Why homeodynamics, not homeostasis?, *The Scientific World Journal* 1 (2001) 133–145. doi:10.1100/tsw.2001.20.
- [53] R. Thomas, Laws for the dynamics of regulatory networks, *Int J Dev Biol* 42 (3) (1998) 479–485. doi:10.1387/IJDB.9654035.
- [54] L. Glass, A. Beuter, D. Larocque, Time delays, oscillations, and chaos in physiological control systems, *Math Biosci* 90 (1) (1988) 111–125. doi:10.1016/0025-5564(88)90060-0.
- [55] L. Glass, C. Malta, Chaos in multi-looped negative feedback systems, *J Theor Biol* 145 (2) (1990) 217–223. doi:10.1016/S0022-5193(05)80127-4.

The effect of integral control in oscillatory and chaotic reaction kinetic networks

Supplementary Material

Kristian Thorsen^a, Tormod Drengstig^a, Peter Ruoff^b

^a *Department of Electrical Engineering and Computer Science, University of Stavanger, Norway*

^b *Centre for Organelle Research, University of Stavanger, Norway*

SM1: Control of average concentration against different inflow disturbances during oscillations

Figure S1 shows the results of a full sweep study of the average level of A versus the strength of inflow disturbance, k_p^i , for the outflow controller in Fig. 2a in the main text. Simulations are run for different levels of inflow disturbance k_p^i and the averages of A and E are calculated. The periodic average of A , $\langle A \rangle$, is maintained near $\langle A \rangle_{set} = k_6/k_5$ (see Eq. 12 in the main paper). The actual average level is somewhat lower than the theoretical setpoint because K_M^E is relatively large in this example ($K_M^E = 0.5$); refer to section 2.1 of the main paper for an explanation. This is particularly the case for low values of E where $f(E)$ is significantly lower than 1. Aside from this, the average level of A is as good as independent of the disturbance.

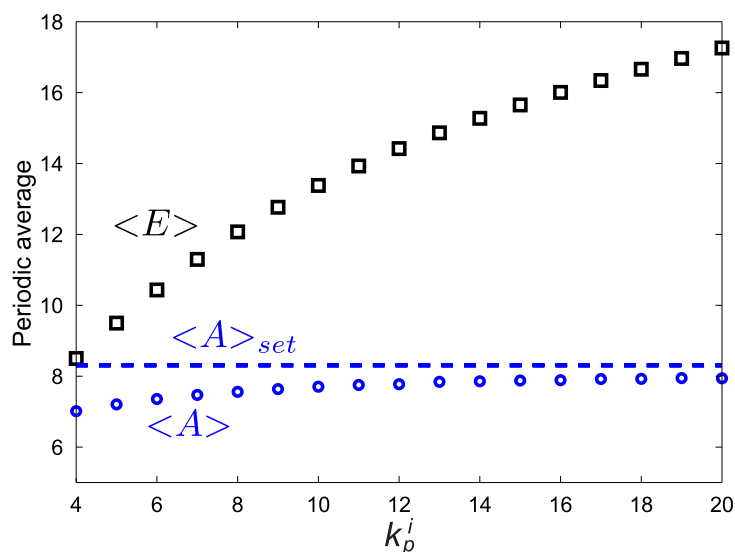


Figure S1: **Control of the periodic average of A under oscillatory conditions.** Periodic average level of A , $\langle A \rangle$ (blue circles) for the oscillatory outflow controller in Fig. 2a (Eqs. 5 and 1). The black squares show the periodic average of E , and the dashed blue line shows the theoretical setpoint of A , $\langle A \rangle_{set} = k_6/k_5 = 8.3$. Parameters: $k_2 = 1.5$, $k_3 = 3.8$, $k_5 = 0.65$, $k_6 = 5.4$, $K_M^A = 0.15$, and $K_M^E = 0.5$. Initial conditions: $A_0 = 25.95$, $E_0 = 7.63$. Transient effects are avoided by letting simulations run for a time length of 100 before starting to calculate the averages.

SM2: Flow in phase space and reinjection in the chaotic outflow controller

Figure S2 shows how reinjection happens in the chaotic outflow controller. The manifold created by the fast dynamics in the Z -variable (Eq. 16 in the main paper) divides the phase space into a region with downward and a region with upward flow in the Z -direction, as shown in Fig. S2a. When the oscillations pass over the switch threshold and into the area with upward flow they are guided by the manifold upwards in phase space. As they move upward they reach a region where the flow is reversed, as shown in Fig. S2b. The reversed flow brings the trajectories over the slow manifold and into the region with downward flow. The trajectories move down and are reinjected into the spiralling oscillator. What actually makes the reversed flow is the $k_4AZ/(K_{M,2}^A + A)$ part in the equation for \dot{A} (Eq. 13 in the main paper).

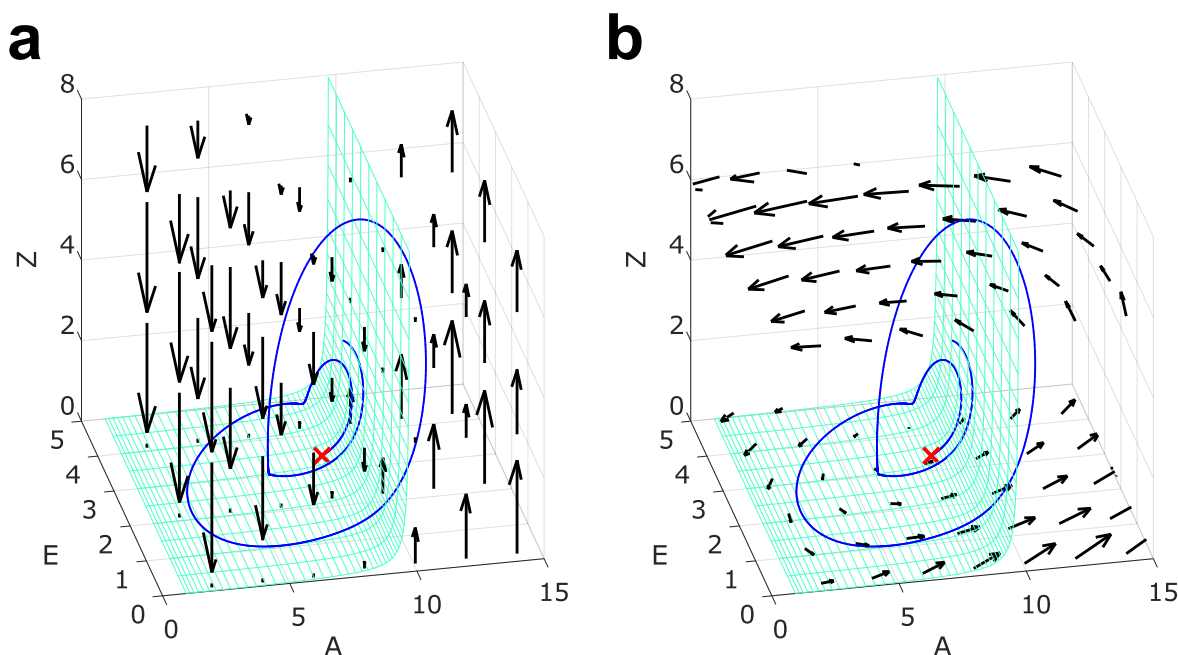


Figure S2: **Slow manifold and direction of flow in phase space for the chaotic outflow controller.** (a) Manifold created by the fast dynamics in the Z -variable (green), example trajectory (blue), and arrows showing the flow in Z -direction (black). The manifold divides the phase space into a region with downward flow and a region with upward flow. (b) Manifold created by the fast dynamics in the Z -variable (green), example trajectory (blue), and arrows showing the flow in AE -direction (black). There is reversed flow already for $Z = 6$. Parameters: $k_p^i = 4$, $k_2=1.5$, $k_3=3.8$, $k_4=3.7$, $k_5=0.65$, $k_6=5.4$, $k_7=7.7$, $k_8=75$, $K_{M,1}^A=K_{M,2}^A=0.15$, $K_M^E=0.5$, and $K_M^Z=0.03$. The trajectory starts in $[5.5, 4.5, 0.04]$ (red cross).

A comment about the F -manifold created by the fast dynamics in Z (Eq. 16 in the main paper): This surface only guides the slow movement of the trajectories. The faster the dynamics in Z compared to the dynamics in the rest of the system, the closer the trajectories will be to this surface. The trajectories will move exactly on the surface in the limit case when the dynamics in Z are instant. In that case we will have a 2D oscillator moving on the surface and there will no longer be chaos.

SM3: Movie – Poincaré sections, first-return maps, and movement of the attractor in phase space for the chaotic outflow controller

Refer to movie file: [SM3.mp4](#).

As part of our analysis of the extended outflow controller (Fig. 4a in the main text) we recorded the chaotic attractor’s position and shape in phase space for bifurcations in the inflow disturbance, k_p^i , from 1 to 20, i.e., over the same range as shown in the bifurcation diagram in Fig. 4d in the main text. The results are collected in the movie [SM3.mp4](#), which shows how the attractor evolves as k_p^i increases. Each frame in the movie consists of four plots, as shown in Fig. S3 and explained in the following.

The two upper plots (Fig. S3) show the attractor in phase space and its projection into the AE -plane. The attractor changes shape and position as k_p^i increases, but its center of mass appears to stay in the same position relative to the A -axis. This illustrates the effect of integral control; by keeping the average of A at a setpoint, the controller locks the attractor’s position on the A -axis.

A half-plane (black and green) is drawn together with the attractor on the two upper plots in the movie. This is used to create the Poincaré section and first-return maps shown in the two lower plots in the movie. Poincaré sections and first-return maps are convenient tools to analyze (chaotic) attractors. The half plane is defined by,

$$0 < A < 6.5, \quad E = \frac{9k_p^i}{32} + \frac{19}{8}, \quad 0 < Z < 7, \quad (\text{S1})$$

so that it always is placed in a part of the attractor where no folding takes place and where all intersections with this half plane are from the same side [43]. The Poincaré section (lower left plot in the movie) shows where trajectories cross the half plane. Periodic oscillations produce one (e.g., $k_p^i = 1.1$), or several (e.g., $k_p^i = 3$), distinct points on this plot as the trajectory always cross the half plane in the same places. (This point often looks like a straight line in the movie due to auto-scaling of the axis.) Chaotic oscillations on the other hand shows up as a bent curve, e.g., $k_p^i = 9.15$, as shown in Fig. S3 (lower left).

The Poincaré section is also used to draw the first-return map which is shown in the lower right plot in the movie. The first-return map reveals how intersection $n+1$ of the Poincaré section depends on intersection n . Chaotic attractors are often characterized by the appearance of their first-return maps [42, 43]. We will not go into further detail here than to note that the first-return map change in appearance for different chaotic values of k_p^i . A value of $k_p^i = 3.45$ produces a unimodal map with two monotonic branches that meets in a minimum point, whereas $k_p^i = 9.15$ produces a multimodal map as shown in Fig. S3 (lower right).

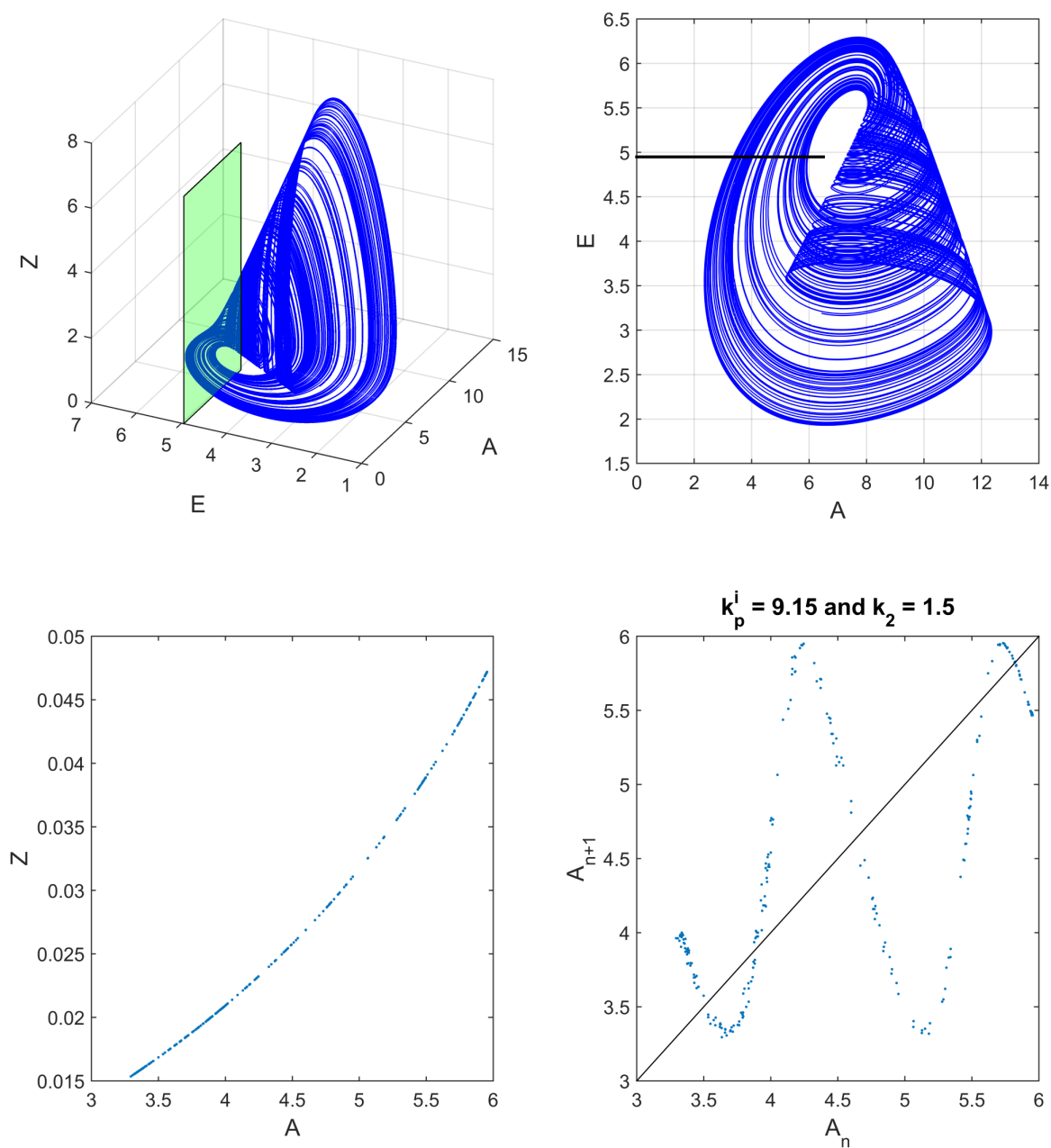


Figure S3: **Overview of plots shown in the movie SM3.mp4.** The movie runs at two frames per second and each frame shows the results from one simulation with a particular value for the inflow disturbance k_p^i , which is changed in steps of 0.05 from frame to frame. The other parameters are: $k_2=1.5$, $k_3=3.8$, $k_4=3.7$, $k_5=0.65$, $k_6=5.4$, $k_7=7.7$, $k_8=75$, $K_{M,1}^A=K_{M,2}^A=0.15$, $K_M^E=0.5$, $K_M^Z=0.03$. Each simulation is started with $A_0=8.30$, $E_0=3.18$, and $Z_0=0.16$ as initial conditions, but allowed to run for 500 time units before plotting to avoid startup transients. The plot in the upper left position shows the attractor in phase space and a half plane given by $E = (9/32)k_p^i + 19/8$, $0 < A < 6.5$, $0 < Z < 7$. The plot in the upper right position shows the projection in AE -space. The plot in the lower left position shows the Poincaré section where the trajectories cross through the half plane, and the plot in the lower right position shows the corresponding first-return map.

SM4: The setpoint for the chaotic outflow controller and its connection to the equilibrium point of the system

As done for the Brusselator in section 3.3 of the main text, it is also possible to relate the setpoint of $\langle A \rangle_\tau$ and the behavior of $\langle E \rangle_\tau$ for the chaotic outflow controller to an unstable equilibrium point of the overall system. The system equations for the chaotic outflow controller are repeated below (Eqs. 13–15 in the main paper):

$$\dot{A} = k_p^i + k_2 A - \frac{k_3 A E}{K_{M,1}^A + A} - \frac{k_4 A Z}{K_{M,2}^A + A} \quad (\text{S2})$$

$$\dot{E} = k_5 A - \frac{k_6 E}{K_M^E + E} \quad (\text{S3})$$

$$\dot{Z} = k_7 A - \frac{k_8 Z}{K_M^Z + Z}. \quad (\text{S4})$$

We could potentially find all possible equilibrium points for this system by setting the left hand side equal to zero and solving the resulting equations. Unfortunately it is difficult to find an explicit analytical solution without making some simplifications. We are here only interested in the equilibrium point that has its A coordinate equal to the setpoint, and will therefore consider the ideal case where E acts as a perfect integral controller, i.e., assume that $K_M^E \ll E$. This holds pretty well for the parameters we use, and better and better as k_p^i increases, see the SM3 movie (top panels). Using this assumption and setting Eq. S3 equal to zero gives:

$$A^* = \frac{k_6}{k_5}. \quad (\text{S5})$$

It is tempting to use the same assumption for Z , i.e., that $K_M^Z \ll Z$. This would lead to an additional explicit value for A^* , something which is problematic. The assumption that $K_M^Z \ll Z$ does however not hold for the parameter values that we use. The value of Z stays close to K_M^Z for a large portion of the time, as can be seen in the trajectories in the SM3 movie. Solving Eq. S4 for Z ($\dot{Z} = 0$) and inserting A^* from above gives:

$$Z^* = \frac{k_7 A^* K_M^Z}{k_8 - k_7 A^*} = \frac{k_7 \left(\frac{k_6}{k_5}\right) K_M^Z}{k_8 - k_7 \left(\frac{k_6}{k_5}\right)}. \quad (\text{S6})$$

Solving Eq. S2 for E^* ($\dot{A} = 0$)

$$E^* = \frac{k_p^i}{k_3} \left[\frac{K_{M,1}^A + A^*}{A^*} \right] + \frac{k_2}{k_3} [K_{M,1}^A + A^*] - \frac{k_4}{k_3} Z^* \left[\frac{K_{M,1}^A + A^*}{K_{M,2}^A + A^*} \right], \quad (\text{S7})$$

and then inserting A^* and E^* from Eqs. S5 and S6 gives:

$$E^* = \frac{k_p^i}{k_3} \left[\frac{K_{M,1}^A + \left(\frac{k_6}{k_5}\right)}{\left(\frac{k_6}{k_5}\right)} \right] + \frac{k_2}{k_3} \left[K_{M,1}^A + \left(\frac{k_6}{k_5}\right) \right] - \frac{k_4}{k_3} \left[\frac{k_7 \left(\frac{k_6}{k_5}\right) K_M^Z}{k_8 - k_7 \left(\frac{k_6}{k_5}\right)} \right] \left[\frac{K_{M,1}^A + \left(\frac{k_6}{k_5}\right)}{K_{M,2}^A + \left(\frac{k_6}{k_5}\right)} \right]. \quad (\text{S8})$$

Note that the actual position of this equilibrium point will differ slightly in the practical case, depending on the value of K_M^E . We have seen in the main text that the equilibrium is unstable. However, the results in the main paper has shown that the average level of A is kept close to A^* (Fig. 5), and we will thus expect the same for the average value of E and Z . As shown in Fig. S4,

this is indeed the case. Looking at Fig. S4b and on the first term in Eq. S8 we clearly see how the average level of E increases proportionally to the level of inflow disturbance.

The difference between $\langle A \rangle_\tau$ and the theoretical setpoint can be attributed to the level of E and the parameter K_M^E . E increases with k_p^i and the removal of E becomes more saturated. The $f(E)$ fraction (see section 2.1 in the main text) gets closer to 1 and the controller operates more and more like a perfect integral controller.

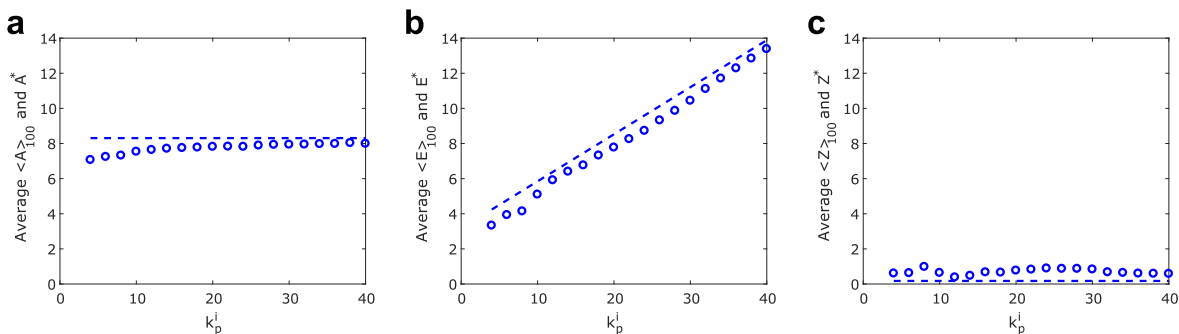


Figure S4: **Average levels and ideal equilibrium point.** Average levels (blue circles) of the three state variables in the chaotic outflow controller (Eqs. S2-S4) plotted together with the ideal equilibrium point (A^* , E^* , Z^*) (dashed blue lines) for different levels of inflow disturbances. (a) Average level of A , $\langle A \rangle_{100}$, and A^* (Eq. S5). (b) Average level of E , $\langle E \rangle_{100}$, and E^* (Eq. S8). (c) Average level of Z , $\langle Z \rangle_{100}$, and Z^* (Eq. S6). The averages are calculated over a time length of $\tau=100$. Parameters: $k_2=1.5$, $k_3=3.8$, $k_4=3.7$, $k_5=0.65$, $k_6=5.4$, $k_7=7.7$, $k_8=75$, $K_{M,1}^A=K_{M,2}^A=0.15$, $K_M^E=0.5$, and $K_M^Z=0.03$. Initial conditions: $A_0=8.30$, $E_0=3.18$ and $Z_0=0.16$. Transient effects are avoided by letting simulations run for a time length of 100 before calculating the averages.

SM5: Averaging over successive intersections of a Poincaré section

Since chaotic systems do not have a defined period we calculated the average over a specific length of time τ in the main paper. This method is convenient, easy, and works well, but it is arguably not as elegant as the calculation of the periodic average. An alternative approach that is more equivalent to the periodic average is to calculate the average between two successive intersections with a Poincaré section. We have done this for the same experiment as shown in Fig. 6 in the main paper, and the results are shown in Fig. S5 on the following page. We have here used the Poincaré plane given in Eq. S1, and its placement is shown in Fig. S5d–f. Each crossing of the Poincaré plane is detected and marked with a red asterisk on the time series of A , E , and Z in the figure. The average between two successive crossings is calculated by taking the integral of the signal divided by the time between the crossings.

The results are similar to what is shown in the main paper. Both the average of A over a specific length of time, and the average of A between two successive crossings of the Poincaré plane, are kept constant despite disturbances (changes in the inflow parameter k_p^i).

We selected not to use this Poincaré section based method for the results presented in the main paper. This is because the method is cumbersome as the attractor has to be manually inspected to make sure that the corresponding Poincaré plane is placed in a part of the attractor where no folding takes place, and where all intersections with the Poincaré plane is from the same side [43]. A new Poincaré plane thus has to be defined for each different system, and for each different set of parameters. It may furthermore also be necessary to move the Poincaré plane as the system is perturbed by disturbances, as these are changes in parameter values that cause the attractor to move and change shape (see SM3). This makes this method inconvenient to use; especially for studies where one wants to do a large sweep over different parameter values.

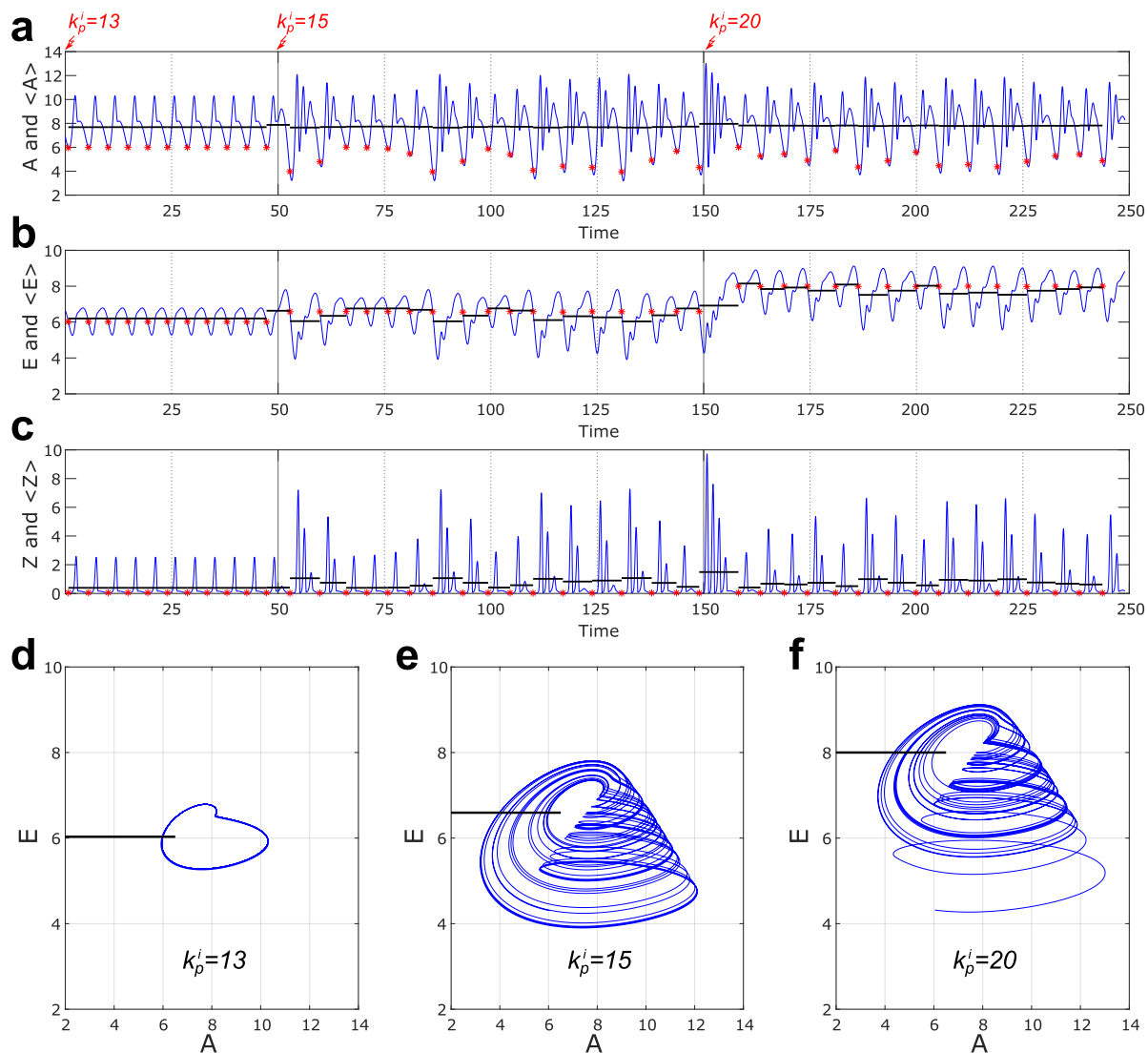


Figure S5: **Example response for the chaotic outflow controller to a stepwise change in inflow with averages calculated between successive crossings of a Poincaré plane.**

(a) Response to an inflow disturbance given as a stepwise change for the chaotic outflow controller in Fig. 4a (Eqs. 13-15 in the main text). The disturbance k_p^i is stepped from 13 to 15 at $t=50$, and from 15 to 20 at $t=150$, as indicated. The level of A is shown in blue while the average of A , $\langle A \rangle$, calculated between successive crossings of a Poincaré plane (marked with red asterisks) is shown in black. (b) Level and average of E . (c) Level and average of Z . Parameters: $k_2=1.5$, $k_3=3.8$, $k_4=3.7$, $k_5=0.65$, $k_6=5.4$, $k_7=7.7$, $k_8=75$, $K_{M,1}^A=K_{M,2}^A=0.15$, $K_M^E=0.5$, and $K_M^Z=0.03$. Initial conditions: $A_0=6.91$, $E_0=6.65$ and $Z_0=0.07$. (d-f) Placement of the Poincaré plane used, and the shape of the attractor for different k_p^i values.

SM6: Effect of integral action in an inflow controller

The second motif used in this study is an inflow controller (type 2 in [4]) shown in Fig. S6. The reaction network for the controller part, E , is the same as in the outflow controller, but instead of acting on the outflow of A it acts on the inflow. Also, since this controller compensates with an inflow it is natural that the disturbance is an outflow (k_p^o). The overall negative feedback in this motif is achieved by E inhibiting the inflow of A (with inhibition constant K_I^E). Thus, an increase in E will decrease the compensatory inflow of A . Except for the difference in how these motifs act on A they both have integral control of A as long as the removal of E is close to zero-order ($K_M^E \ll E$).

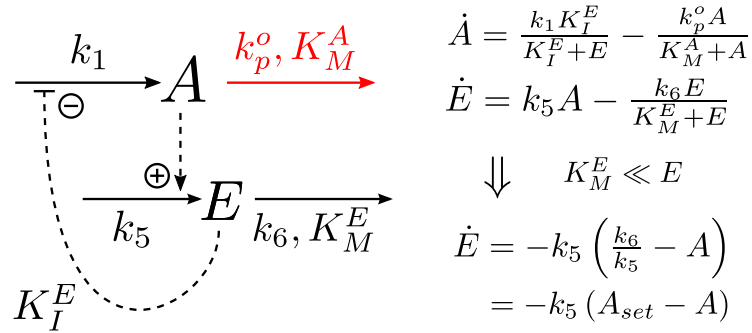


Figure S6: **Negative feedback inflow controller.** Reaction network representation and rate equations for the motif. The controller variable E is activated by A and feeds back by inhibiting the inflow of A .

Periodic oscillations

Oscillations are in this controller achieved by having an extra component a in series with A . The reaction kinetic network is shown in Fig. S7a, and the rate equations for this system are:

$$\dot{a} = \frac{k_1 K_I^E}{K_I^E + E} - \frac{k_2 a}{K_M^a + a} \quad (\text{S9})$$

$$\dot{A} = \frac{k_2 a}{K_M^a + a} - \frac{k_p^o A}{K_M^A + A} \quad (\text{S10})$$

$$\dot{E} = k_5 A - \frac{k_6 E}{K_M^E + E}. \quad (\text{S11})$$

This controller can provide robust control of A under both stationary and oscillatory conditions. The rate constant k_p^o represents the outflow disturbance of A . The controller species E varies according to changes in k_p^o and adjusts the compensatory flux $j = k_1 K_I^E / (K_I^E + E)$ by inhibition (with inhibition constant K_I^E).

Figures S7b-S7d show the oscillatory behavior in a , A and E for a stepwise change in k_p^o . The regulation of the periodic average in A , $\langle A \rangle$, can be seen by the straight black line in Fig. S7c. The periodic average of A is robustly maintained at $\langle A \rangle \approx 10.3$ and is near independent of the disturbance. The level of $\langle A \rangle$ is only somewhat lower than the theoretical setpoint, i.e. $k_6/k_5 = 10.77$. This motif shows a more accurate, or perfect, control than the one in the main text; the inaccuracy is lower compared to the outflow motif with autocatalysis. The explanation behind this difference is as follows: The oscillatory behavior and maximum level of E in Fig. S7d

is comparable to the behavior and level of E in Fig. 3b. The value of K_M^E in the two examples are, however, different at 0.01 and 0.5. This affects the $f(E)$ factor (see Eq. 4), and thus the controller accuracy.

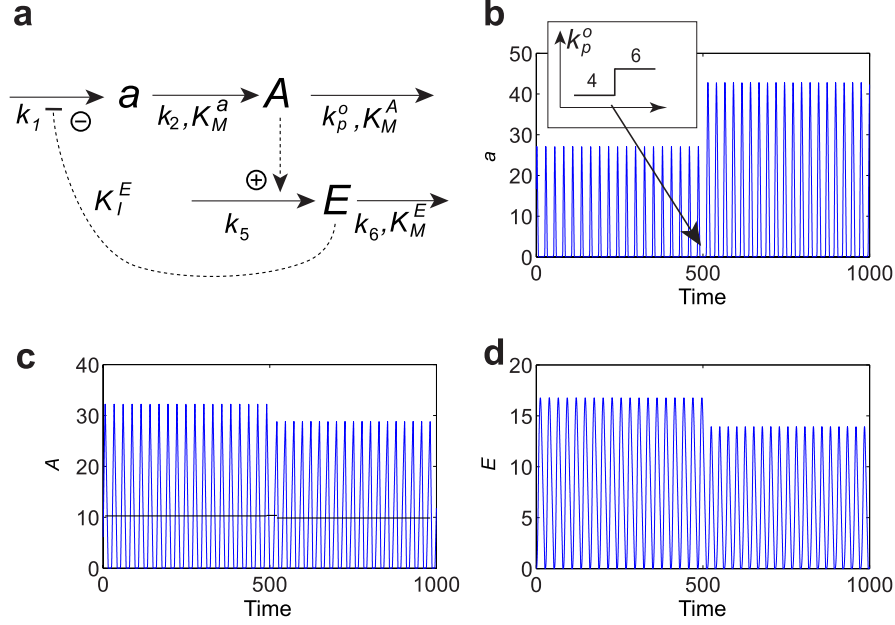


Figure S7: **Negative feedback inflow controller with oscillatory behavior.** (a) Inflow controller of third order without autocatalysis in A (Eqs. S9–S11). The controller variable E is activated by A and feeds back by inhibiting the inflow of a . (b) Oscillations in a shown for a stepwise outflow disturbance in k_p^o (from 4 to 6 at $t=500$ as indicated). Parameters: $k_1=20$, $k_2=9$, $k_5=0.13$, $k_6=1.4$, $K_I^E=0.2$, $K_M^a=1$, $K_M^A=0.1$, and $K_M^E=0.01$. Initial conditions: $a_0=16.62$, $A_0=6.10$ and $E_0=0.01$. (c) Oscillations in A (blue) and periodic average of A (black) during the experiment. (d) Oscillations in E during the experiment.

Chaotic oscillations

We extend the inflow motif (Eqs. S9–S11) with a Z -component to enable chaos. The overall dimension of this motif is four; a , A , and E makes out the original limit cycle oscillator in three dimensions, and Z is a one dimensional switch. The overall reaction kinetic model is shown in Fig. S8a, and the rate equations are:

$$\dot{a} = \frac{k_1 K_I^E}{K_I^E + E} - \frac{k_2 a}{K_M^a + a} + k_4 Z \quad (\text{S12})$$

$$\dot{A} = \frac{k_2 a}{K_M^a + a} - \frac{k_p^o A}{K_M^A + A} \quad (\text{S13})$$

$$\dot{E} = k_5 A - \frac{k_6 E}{K_M^E + E} \quad (\text{S14})$$

$$\dot{Z} = k_7 - \frac{k_8 Z A}{K_M^Z + Z}. \quad (\text{S15})$$

Notice that A now activates the outflow of Z and that Z activates the inflow of A ; this is the opposite structure compared to how Z is arranged in the outflow controller shown in Fig. 4a.

The dimension of this inflow controller makes it difficult to get an intuitive understanding of how chaos appears. The AEZ -phase space shown in Fig. S8b is an attempt to illustrate the typical chaotic behavior in phase space by using color as a way to encode the fourth state variable a . Trajectories circulate downwards like on a spring that is lying on an incline. They make a small number of rotations with increasing amplitude in A and a until a very high value of a (bright pink in the figure) is reached; this is then followed by a crash into the bottom of phase space with $Z \approx 0$. The trajectories then follow the AE plane ($Z \approx 0$) before they are lifted up by an increasing Z and reinjected at the top of the spring.

Depending on the strength of outflow disturbances, k_p^o , this controller can show both stable, periodic, and chaotic behavior. A bifurcation diagram for a certain set of parameter values is shown in Fig. S8c. The system is asymptotically stable to a point for low values of k_p^o ; it starts to oscillate when $k_p^o \geq 2.02$ and follows a period doubling route to chaos. The system is then mostly chaotic until around $k_p^o = 7.87$ where it again shows periodic oscillations. Increasing k_p^o above 9 will cause the system to become unstable and cause a , E and Z to diverge towards infinity; this happens because the set of parameters used limits the flow from a to A to a maximum of 2 ($k_2 = 2$).

An example of the controller's response to a stepwise increase in outflow is shown in Figs. S8d-S8g. Increasing k_p^o from 4 to 6 causes the system to do a couple of more circulations before each reinjection (seen as more oscillations with increasing amplitude in the time series), but the average level of A is kept constant. Further studies show, as expected, that the average value of A is kept at its setpoint of $k_6/k_5 = 10.77$ over the whole relevant range of outflow disturbances. These results are shown in Fig. S9. The regulation of $\langle A \rangle_{1000}$ is within $\pm 2\%$, highlighting again the importance of K_M^E and $f(E)$. The regulation of $\langle A \rangle$ during chaos is much tighter for this motif with a $K_M^E = 0.01$ than for the autocatalytic motif with a $K_M^E = 0.5$ (Fig. 5). We remark, however, that the small differences between $\langle A \rangle_{1000}$ and the theoretical setpoint, and the variance in this difference seen in Fig. S9, can be attributed to both the level of E and the effect of the $f(E)$ factor, and to the time length used for averaging, ref. Eqs. 20–21.

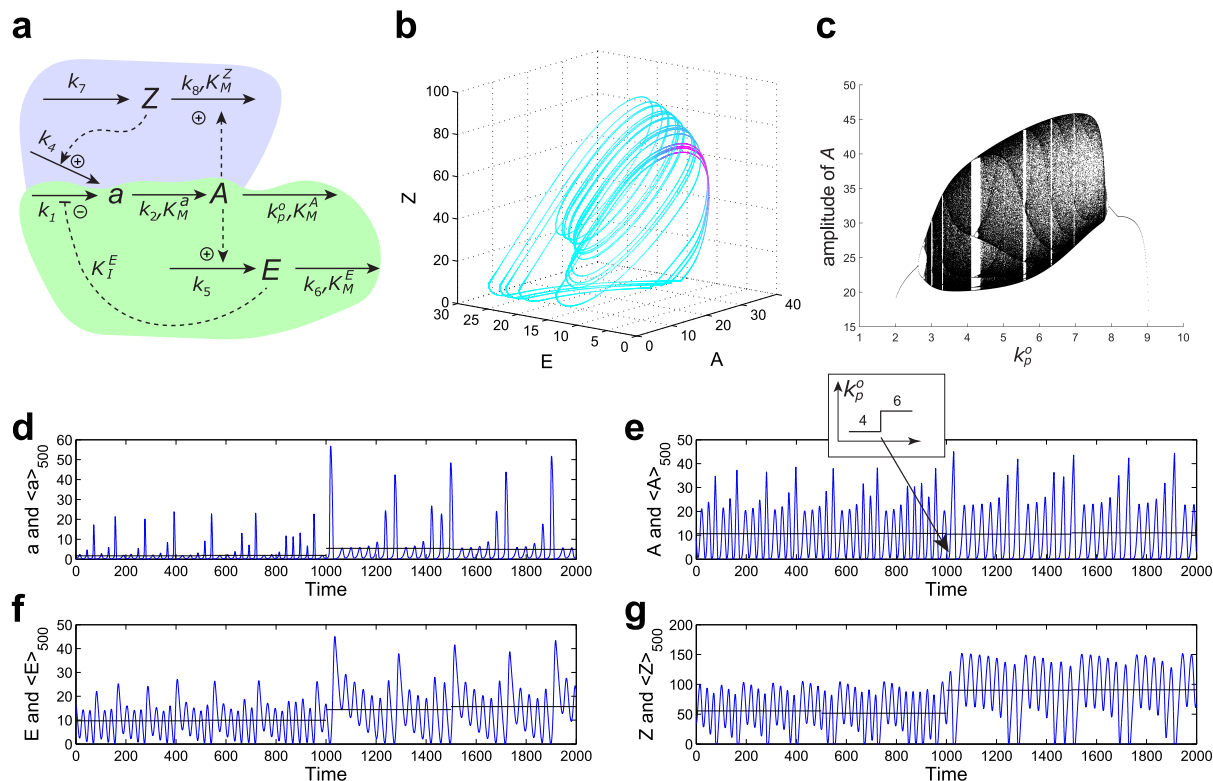


Figure S8: **Extended inflow controller capable of showing chaotic behavior.** (a) Chaotic inflow controller where the green part is identical to the oscillatory model in Fig. S7a, and the blue part is an additional feedback added to enable chaotic behavior. (b) Typical chaotic behavior shown in AEZ -space. The fourth state, a , is encoded as color from cyan ($a=0$) to pink ($a=20$) (linear relationship). Parameters: $k_p^o=4$, $k_1=20$, $k_2=9$, $k_4=0.05$, $k_5=0.13$, $k_6=1.4$, $k_7=7$, $k_8=0.7$, $K_I^E=0.2$, $K_M^a=1$, $K_M^A=0.1$, $K_M^Z=0.1$, and $K_M^E=0.01$. Initial conditions: $a_0=0.26$, $A_0=8.92$, $E_0=16.27$ and $Z_0=33.34$. (c) Bifurcation diagram showing how the amplitude of oscillations in A changes with the strength of the outflow disturbance k_p^o . (Simulations are run for 5000 time units before collecting data to avoid transients.) (d) Response to a disturbance given as a stepwise change in outflow k_p^o (from 4 to 6 at $t=1000$). Chaotic behavior of a shown in blue and average of a , $\langle a \rangle_{500}$ shown in black. (e) Chaotic behavior of A (blue) and average of A , $\langle A \rangle_{500}$ (black). (f) and (g) Chaotic behavior (blue) and averages (black) of E and Z during the experiment. The averages are calculated over fixed intervals with a length of $\tau=500$.

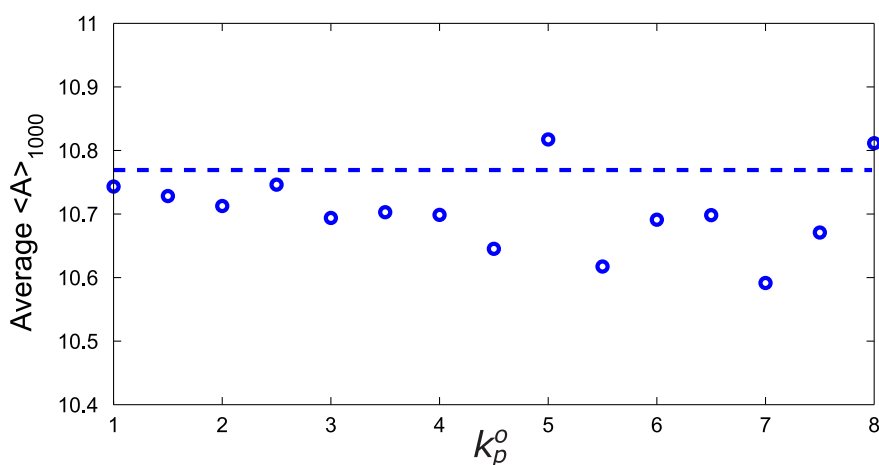


Figure S9: **Control of the average of A under chaotic conditions.** Average level of A , $\langle A \rangle_{1000}$ (blue circles) for the chaotic inflow controller in Fig. S8a (Eqs. S12–S15) for different levels of outflow disturbances. The dashed blue line shows the theoretical setpoint of A , $\langle A \rangle_{set} = k_6/k_5 = 10.77$. The averages are calculated over a time length of $\tau = 1000$. Parameters: $k_1 = 20$, $k_2 = 9$, $k_4 = 0.05$, $k_5 = 0.13$, $k_6 = 1.4$, $k_7 = 7$, $k_8 = 0.7$, $K_I^E = 0.2$, $K_M^a = 1$, $K_M^A = 0.1$, $K_M^Z = 0.1$, and $K_M^E = 0.01$. Initial conditions: $a_0 = 0.26$, $A_0 = 8.92$, $E_0 = 16.27$ and $Z_0 = 33.34$. Transient effects are avoided by letting simulations run for a time length of 1500 before calculating $\langle A \rangle_{1000}$.

SM7: Movie – Trajectories moving on the attractor for the chaotic inflow controller

Refer to movie file: [SM7.mp4](#).

This movie shows an animation of how the trajectories move in phase space for the chaotic inflow controller. The left plot in the movie shows the same AEZ -space as Fig. S8b, with the fourth state, a , linearly encoded as a color from cyan ($a=0$) to pink ($a=20$). The right plot in the movie shows the same results, but plotted in AZa -space with E linearly encoded as a color from cyan ($E=0$) to pink ($E=25$).

SM8: Alternative configuration of a chaotic inflow controller

The two controller motifs of the main text (outflow motif) and the supplementary information (inflow motif) were first extended to exhibit limit cycle type periodic oscillations, and then extended again with a new variable Z to facilitate for the occurrence of reinjection in phase space, and thus chaos. In both examples Z creates a feedback loop through itself and the controlled species A , but is not directly affected by, or directly affects, the original controller species E .

Here we present an alternative configuration where Z instead is affected by E and where Z affects itself by a feedback loop through all the components of the system (a , A and E). This chaotic inflow motif, shown in Fig. S10a, does for a certain set of parameters show a much more spiky behavior than the other two motifs. This system displays a behavior where the controlled variable A shows spikes with about 50-fold higher peak values than the setpoint value, see Fig. S10e. These spikes are however very short in length, and the overall average of A is still defended at its setpoint.

The behavior of this system in phase space is visualized in Fig. S10b. The behavior can be divided into a slow and a fast phase. The movement in the EZ -plane ($A \approx 0$) is slow, seen from the relative slow decay of E and Z in Figs. S10f and S10g. A shift in behavior then occurs when the trajectory in the EZ -plane hits the AZ -plane ($E \approx 0$). There is a rapid spike in a due to the lack of inhibition on its inflow; this spike propagates through the system as a spike in A , and E . The inhibition by E of a is quickly restored, and the concentrations of both a and A drops rapidly back to low values as there is no saturation of the outflow of a and A in this system (the removal of a and A is follows a linear relationship instead of Michaelis-Menten).

The rate equations for this system are:

$$\dot{a} = \frac{k_1 K_I^E}{K_I^E + E} - k_2 a - k_3 a Z \quad (\text{S16})$$

$$\dot{A} = k_2 a - k_p^o A \quad (\text{S17})$$

$$\dot{E} = k_5 A - \frac{k_6 E}{K_M^E + E} \quad (\text{S18})$$

$$\dot{Z} = k_7 - \frac{k_8 Z}{K_M^Z + Z}. \quad (\text{S19})$$

The bifurcation diagram in Fig. S10c shows how this system behaves for different strengths of outflow disturbance (k_p^o) from 1 to 10. Again we see that the system follows a period doubling route to chaos, much like the inflow controller in SM6 (Fig. S8c). Chaos starts at $k_p^o=2.98$, and the system is then mostly chaotic for the rest of the considered range. The peak values of the spikes vary greatly for different k_p^o values. The average level of A is nonetheless kept remarkably stable over this range of outflow disturbances, see Fig. S11. The regulation of $\langle A \rangle$ is actually much tighter than for any of the examples used in the main text. The reason for this is that a very low K_M^E value is used in this example (10^{-6}), which lets E operate very close to a perfect integral controller.

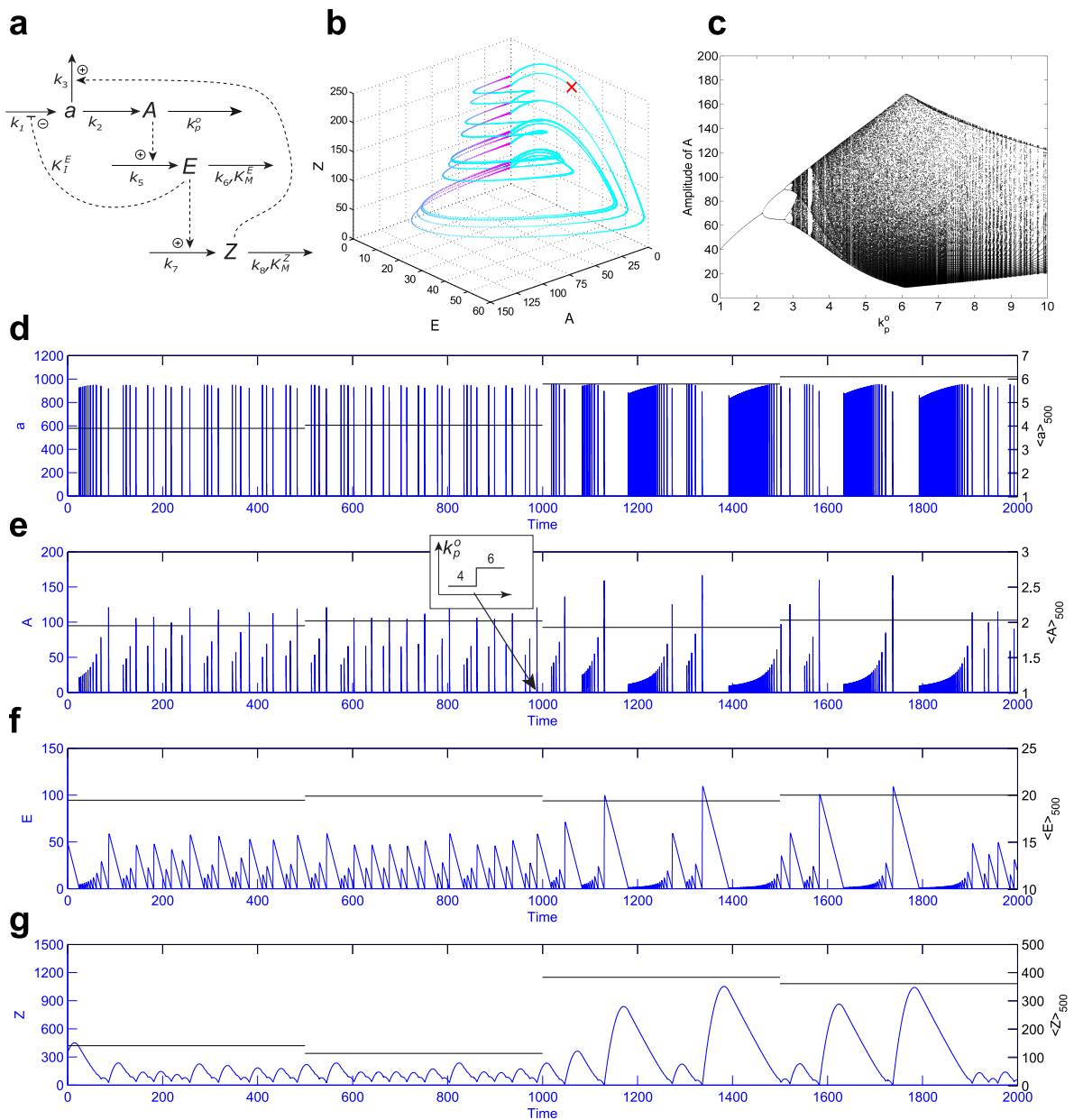


Figure S10: **Alternative configuration of an extended and modified inflow controller showing chaotic behavior.** (a) Chaotic inflow controller extended from the oscillatory aAE motif (Fig. S7a). The controller is extended with an additional species Z , which is affected by E and which acts on a creating a feedback loop through all components of the system. (b) Typical chaotic behavior shown in AEZ -space. The fourth state, a , is encoded as color from cyan ($a=0$) to pink ($a=1000$) (linear relationship). Parameters: $k_p^o=4$, $k_1=10^6$, $k_2=2$, $k_3=0.2$, $k_5=1$, $k_6=2$, $k_7=0.5$, $k_8=10$, $K_I^E=10^{-6}$, $K_M^Z=10^{-7}$, and $K_M^E=10^{-6}$. Initial conditions: $a_0=8.390 \cdot 10^{-4}$, $A_0=4.135 \cdot 10^{-4}$, $E_0=26.51$ and $Z_0=214.54$. (c) Bifurcation diagram showing how the amplitude of oscillations in A changes with the strength of the outflow disturbance k_p^o . Simulations are run for 3000 time units before collecting data to avoid transients. (d–g) Response in a , A , E , and Z (blue) to a disturbance given as a stepwise change in outflow k_p^o (from 4 to 6 at $t=1000$). Note that average values (black) are shown on the right axis. The averages are calculated over fixed intervals with a length of $\tau=500$.

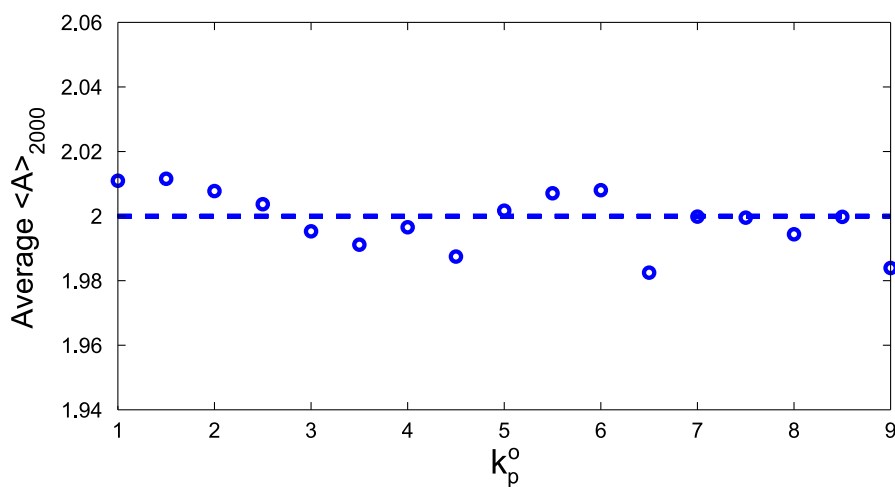


Figure S11: **Control of the average of A under chaotic conditions.** Average level of A , $\langle A \rangle_{2000}$ (blue circles) for the chaotic inflow controller in Fig. S10a (Eqs. S16–S19) for different levels of outflow disturbances. The dashed blue line shows the theoretical setpoint of A , $\langle A \rangle_{set} = k_6/k_5 = 2$. The averages are calculated over a length of $\tau = 2000$ time units. Parameters: $k_1 = 10^6$, $k_2 = 2$, $k_3 = 0.2$, $k_5 = 1$, $k_6 = 2$, $k_7 = 0.5$, $k_8 = 10$, $K_I^E = 10^{-6}$, $K_M^Z = 10^{-7}$, and $K_M^E = 10^{-6}$. Transient effects are avoided by letting simulations run for 3000 time units before calculating $\langle A \rangle_{2000}$.

References

The reference numbers in this SM refers to the reference list in the main paper.